

# Case Study of a 39-Story Building: Model Verification and Performance Comparison with a Semi-active Device

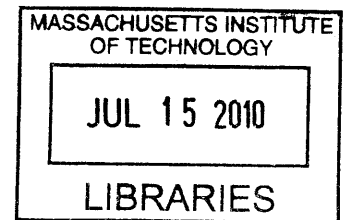
by  
Fernando Pereira-Mosqueira  
Ingeniero de Caminos, Canales y Puertos  
Universidade da Coruña, 2008

**ARCHIVES**

SUBMITTED TO THE DEPARTMENT OF CIVIL AND ENVIRONMENTAL  
ENGINEERING IN PARTIAL FULFILLMENT OF THE REQUIREMENTS FOR THE  
DEGREE OF MASTER OF ENGINEERING IN CIVIL AND ENVIRONMENTAL  
ENGINEERING AT THE MASSACHUSETTS INSTITUTE OF TECHNOLOGY


JUNE 2010

©2010 Fernando Pereira Mosqueira. All rights reserved



The author hereby grants to MIT permission to reproduce and to distribute publicly  
paper and electronic copies of this thesis document in whole or in part in any medium now  
known or hereafter created.

Signature of Author:

  
Department of Civil and Environmental Engineering  
May 14, 2010

Certified by:

  
Jerome J. Connor  
Professor of Civil and Environmental Engineering  
Thesis Supervisor

Accepted by:

  
Daniel Veneziano  
Chairman, Departmental Committee for Graduate Students

Case Study of a 39-Story Building: Model Verification and Performance Comparison with  
a Semi-active Device

By  
Fernando Pereira-Mosqueira

Submitted to the Department of Civil and Environmental Engineering on May 14, 2010 in  
Partial Fulfillment of the Requirements for the Degree of Master of Engineering in Civil  
and Environmental Engineering at the Massachusetts Institute of Technology.

## ABSTRACT

Implementing viscous dampers in high-rise buildings has proven to be an efficient structural way to control interstory drift and accelerations in buildings undergoing wind and earthquake excitations. However, the cost of this implementation sometimes turns to be prohibitive or too high. As a possible more economic solution, this paper introduces the use of a semi-active device to approach this kind of problems. A 39 story building computer model is fully developed. Static and dynamic characteristics of the model obtained are compared with the data obtained from the original design and the wind tunnel results in order to show the accuracy of the computer model. Finally, a comparative study of the efficiency of Modified Friction device and passive dampers under wind excitation is carried out.

Thesis supervisor: Jerome J. Connor

Title: Professor of Civil and Environmental Engineering

## ACKNOWLEDGMENTS

The author would like to acknowledge Dr. Robert McNamara and McNamara/Salvia Inc. for their help with providing data for the simulated structure. The author would also like to thank Simon Laflamme for his help and advice throughout the whole duration of the study. Finally, the author would like to express his gratitude to Professor Jerome J. Connor, Mohamed Abdellaoui Maane, Geoffroy Larrecq, Alexander Graybeal, my parents and Lucia for their help and support at different stages of this thesis.

# CONTENTS

Abstract .....	2
Acknowledgments .....	3
List of figures.....	6
List of tables .....	8
1. Introduction .....	9
1.1. Building structural system.....	9
1.2. Damper characteristics.....	10
2. Viscous dampers (Passive control systems).....	11
2.1. Introduction .....	11
3. Semi-Active Control devices.....	14
3.1. Introduction .....	14
3.2. Variable-Orifice Damper (VOD).....	14
3.3. MagnetoRheological Dampers (MR Dampers).....	15
3.4. Modified friction device (MFD).....	17
4. Control rules for semi-active devices .....	19
4.1. Introduction .....	19
4.2. Linear Quadratic Regulator (LQR).....	20
4.2.1. Clipped optimal rule .....	20
4.3. Sliding mode Controller (lyapunov).....	22
5. Model verification.....	23
5.1. Mass and stiffness matrix extraction methodology .....	23
5.2. Modal analysis comparison .....	24
5.3. Load cases .....	25
5.3.1. Wind load.....	25
5.4. Results.....	26
6. Simulations.....	27
6.1. General strategy.....	27
6.2. MFD 200 kN every 2 stories .....	29
6.3. Heuristic strategy .....	32

6.3.1.	MFD 600 kN every 4 stories .....	33
6.3.2.	MFD 1000 kN every 6 stories .....	35
6.3.3.	MFD 2400 kN every 8 stories .....	37
6.4.	Strategy based on energy dissipation.....	39
6.4.1.	1 <sup>st</sup> iteration (400 kN MFD) .....	39
6.4.2.	2 <sup>nd</sup> iteration (400 kN MFD).....	42
6.4.3.	3 <sup>rd</sup> iteration (800 kN MFD) .....	44
6.4.4.	4 <sup>th</sup> iteration (800 kN MFD) .....	47
6.4.5.	5 <sup>th</sup> iteration (1500 kN MFD) .....	49
7.	Economic evaluation.....	52
8.	Conclusions and further studies.....	54
9.	References .....	55
	Appendix A (viscous damper bracing scheme).....	56
	Appendix B (building structural properties) .....	57

## LIST OF FIGURES

Fig. 1 General viscous damper scheme (R. a. McNamara 2003) .....	9
Fig.2 Detailed viscous damper scheme (R. a. McNamara 2003) .....	10
Fig. 3 Viscous damper and diagonal framing conceptualization.....	11
Fig. 4 Detailed viscous damper scheme (content.answers.com s.f.) .....	11
Fig. 5 Dashpot response under periodic excitation	
Fig. 6 Coulomb device under periodic excitation.....	12
Fig. 7 Coulomb and dashpot system under periodic excitation.....	12
Fig. 8. VOD conceptual model extracted from (Connor 2002).....	14
Fig. 9 Scheme for a MR damper (Choi 2001).....	15
Fig. 10 MR damper and diagonal framing conceptualization .....	15
Fig. 11 MR Damper response under sinusoidal loading (Larrecq 2010).....	16
Fig. 12 MFD Duo-Servo drum brake scheme (Laflamme 2010) .....	17
Fig. 13 MFD conceptualization (Laflamme 2010).....	17
Fig. 14 MFD damper response under sinusoidal loading (Abdellaoui 2010) .....	18
Fig. 15. Flowchart for a controlled system.....	19
Fig. 16 Clipped rule decision scheme .....	21
Fig. 17. SAP2000 structural model for the X and Y directions .....	23
Fig. 18. Stiffness extraction from a 3D frame model for the X direction .....	24
Fig. 19. Periods of vibration for the lumped model.....	25
Fig. 20 Wind load time history.....	26
Fig. 21 Maximum acceleration profile for X direction.....	30
Fig. 22 Maximum acceleration profile for Y direction.....	31
Fig. 23 Viscous damper behavior between 17 <sup>th</sup> and 18 <sup>th</sup> floor for X Direction .....	31
Fig. 24 MFD behavior between 17 <sup>th</sup> and 18 <sup>th</sup> floor X Direction .....	32
Fig. 25 Maximum acceleration profile for X direction.....	33
Fig. 26 Maximum acceleration profile for Y direction.....	34
Fig. 27 MFD behavior between 17 <sup>th</sup> and 18 <sup>th</sup> floor X Direction .....	34
Fig. 28 Maximum acceleration profile for X direction.....	35
Fig. 29 Data Maximum acceleration profile for Y direction.....	36

Fig. 30 MFD behavior between 17 <sup>th</sup> and 18 <sup>th</sup> floor X Direction .....	36
Fig. 31. Maximum acceleration profile for X direction.....	37
Fig. 32. Data Maximum acceleration profile for Y direction.....	38
Fig. 33. MFD behavior between 17 <sup>th</sup> and 18 <sup>th</sup> floor X Direction .....	38
Fig. 34. Maximum acceleration profile for X direction.....	40
Fig. 35. Data Maximum acceleration profile for Y direction.....	41
Fig. 36. MFD behavior between 17 <sup>th</sup> and 18 <sup>th</sup> floor X Direction .....	41
Fig. 37. Data Maximum acceleration profile for X direction.....	43
Fig. 38. Data Maximum acceleration profile for Y direction.....	43
Fig. 39. MFD behavior between 17 <sup>th</sup> and 18 <sup>th</sup> floor X Direction .....	44
Fig. 40. Data Maximum acceleration profile for X direction.....	45
Fig. 41. Data Maximum acceleration profile for Y direction.....	46
Fig. 42. MFD behavior between 17 <sup>th</sup> and 18 <sup>th</sup> floor X Direction .....	46
Fig. 43. Data Maximum acceleration profile for X direction.....	48
Fig. 44. Data Maximum acceleration profile for Y direction.....	48
Fig. 45. MFD behavior between 19 <sup>th</sup> and 20 <sup>th</sup> floor X Direction .....	49
Fig. 46. Data Maximum acceleration profile for X direction.....	50
Fig. 47. Data Maximum acceleration profile for Y direction.....	50
Fig. 48. MFD behavior between 19 <sup>th</sup> and 20 <sup>th</sup> floor X Direction .....	51
Fig. 49. MFD final layout for X and Y direction.....	53

## LIST OF TABLES

Table 1. Damping distribution in the current design .....	10
Table 2. Data extracted from (R. a. McNamara 2003) .....	24
Table 3. Data obtained from the lumped model .....	25
Table 4. Data extracted from (R. a. McNamara 2003) and data obtained from the lumped model.....	26
Table 5. Data obtained from the lumped model .....	29
Table 6. Work done by the MFD's .....	29
Table 7. Work done by viscous damper scheme .....	30
Table 8. Data obtained from the lumped model .....	33
Table 9. Data obtained from the lumped model .....	35
Table 10. Data obtained from the lumped model .....	37
Table 11. Data obtained from the lumped model .....	39
Table 12. Work done by the MFD's .....	40
Table 13. Data obtained from the lumped model .....	42
Table 14. Work done by the MFD's .....	42
Table 15. Data obtained from the lumped model .....	44
Table 16. Work done by the MFD's .....	45
Table 17. Data obtained from the lumped model .....	47
Table 18. Work done by the MFD's .....	47
Table 19. Data obtained from the lumped model .....	49
Table 20. Work done by the MFD's .....	49
Table 21. Economic evaluation chart for heuristic method .....	52
Table 22. Economic evaluation based on the work measurement method .....	53



# 1. INTRODUCTION

## 1.1. BUILDING STRUCTURAL SYSTEM

As McNamara described in his paper (R. a. McNamara 2003), the 39-story building can be considered as a moment-frame-tube structural system. In addition to that, diagonal dampers have been placed on every other floor between the 5<sup>th</sup> and the 34<sup>th</sup> floor in the X direction (E-W). Regarding the Y direction (N-S), toggle braced damper (TBD) was chosen as the appropriate scheme. The main reason to use TBD was the amplification of the damper stroke achieved and the magnification of the damper maximum capacity.

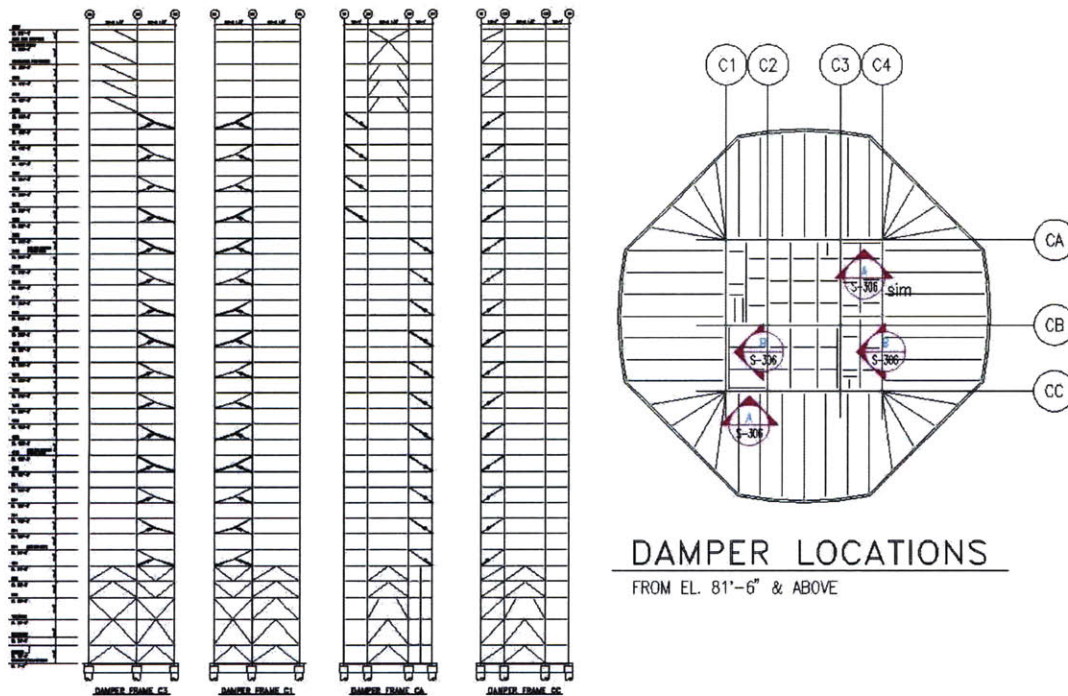


Fig. 1 General viscous damper scheme (R. a. McNamara 2003)

## 1.2. DAMPER CHARACTERISTICS

In the next figure from (R. a. McNamara 2003), it is showed the detailed damping implementation for both directions. Both drawings show the connection between damper and the rest of the structure. The design of those connections is fundamental because they need to transfer the loads to the rest of the structure.

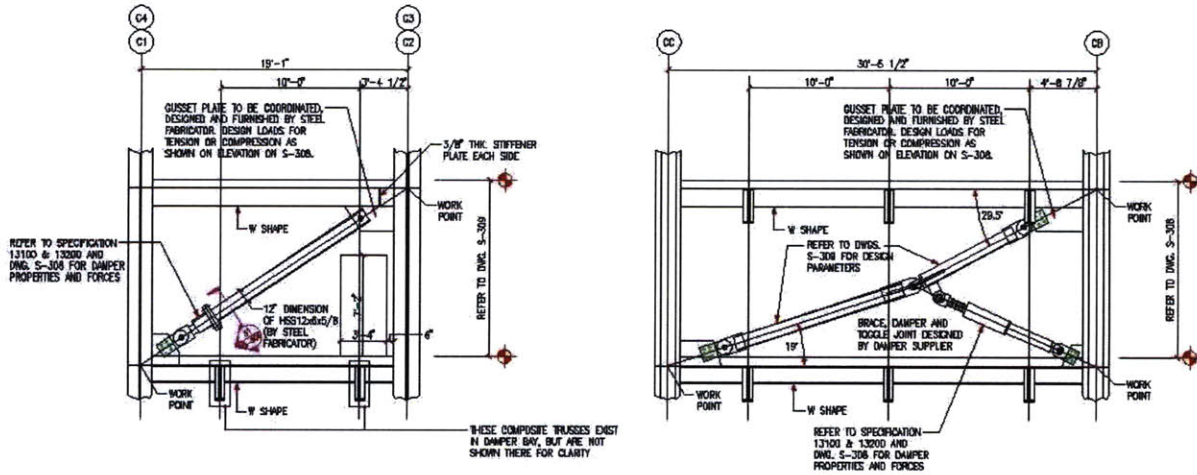


Fig.2 Detailed viscous damper scheme (R. a. McNamara 2003)

In the next table is shown a summary of the total viscous coefficient  $C$  ( $\text{kN*s/m}$ ) per floor and direction. For further description in terms of maximum stroke per floor and bracing angles go to Appendix A. In the following chapter 2, the definition for viscous coefficient is presented.

Floors	$C_x$ total ( $\text{kN/m*s}$ )	$C_y$ total ( $\text{kN/m*s}$ )
5th to 24th	73904	50165
25th to 34th	49270	25082

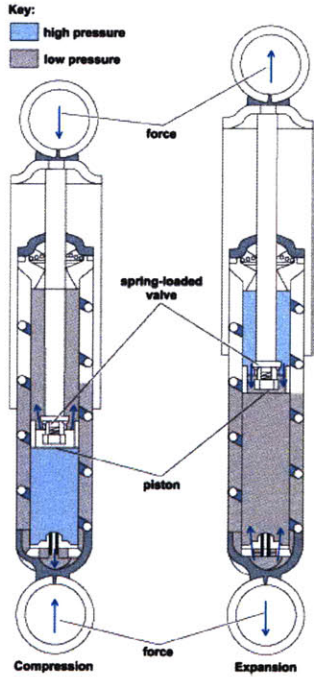
Table 1. Damping distribution in the current design

Next chapter describes in depth the nature of viscous dampers (Fig.4) previously described. Furthermore, a conceptual model is developed (Fig.3) and the behavior of this device is described in Fig.5 to Fig.7.

## 2. VISCOUS DAMPERS (PASSIVE CONTROL SYSTEMS)

### 2.1. INTRODUCTION

Passive control systems, such as viscous dampers, alleviate energy dissipation demand on the primary structure by reflecting or absorbing part of the input energy, thereby reducing possible structural damage (Housner 1997). Specifically, viscous fluid dampers dissipate



energy by turning kinetic energy (due to velocity) into heat. As it can be observed in Fig.3, fluid viscous dampers consist of a piston that moves within a cylinder filled with a viscous fluid that dampen and control motion. A conceptualization of the real model is showed in Fig. 4.

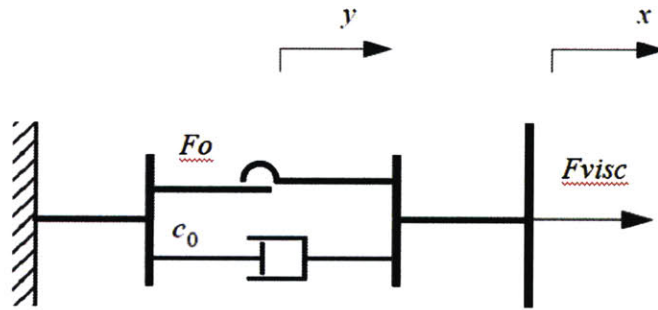


Fig. 3 Viscous damper and diagonal framing conceptualization

Fig. 4 Detailed viscous damper scheme (content.answers.com s.f.)

In regards to the conceptual model, one dashpot is the part causing reduction in the kinetic energy while Coulomb/friction stabilizes the behavior of the damper when velocities are close to zero. This friction damper has capacity one or two orders of magnitude smaller than the viscous damper and it can be neglected most of the times.

$$F_{visc} = c_0 * v^\alpha + F_0 * sign(v) \quad (2.1.)$$

Using this conceptual model, plots of force versus displacement were generated (Fig.5 to Fig.7).

Several graphs are showed to illustrate the viscous damper behavior under periodic excitation and the effect of the friction damper on the general behavior of the system.

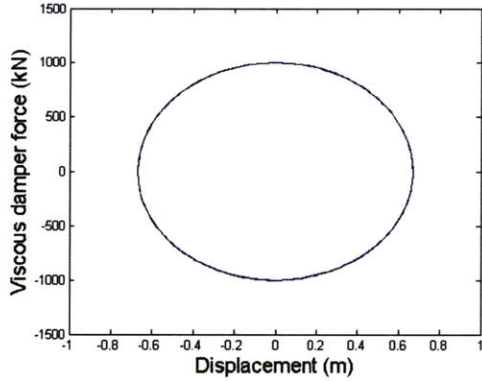


Fig. 5 Dashpot response under periodic excitation

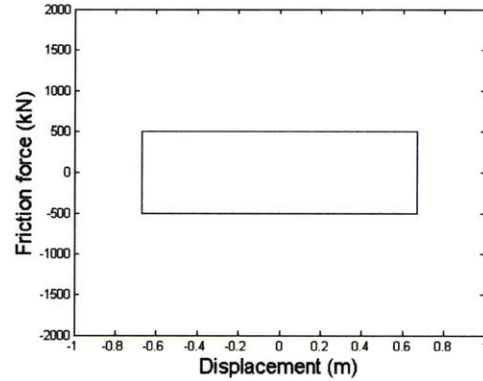


Fig. 6 Coulomb device under periodic excitation

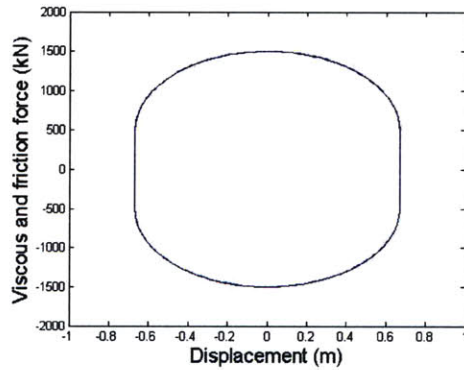


Fig. 7 Coulomb and dashpot system under periodic excitation

Fig. 7 shows the behavior of the model including a dashpot and a friction device. It is important to point out that the friction device adds certain force to the system when displacement is maximum (dashpot is not able to generate any force in this situation of maximum displacements, Fig. 5). The quantity of force generated by the friction model is, as previously mentioned, one or two orders of magnitude smaller than the dashpot maximum capacity. Hence, the transition of the system through velocities equal to zero is still smooth without the discontinuity that a big friction would generate Fig.7.

Viscous dampers are classified as passive devices as previously mentioned. Hence, it is interesting to study some kind of devices able to either exert a force into the structure (active devices) or change their characteristics (semi-active devices) depending on the state of the structure. The latter kind of devices is discussed in the following chapter.

### 3. SEMI-ACTIVE CONTROL DEVICES

#### 3.1. INTRODUCTION

Active control devices have showed to be a more efficient way to dampen structural response under extreme events (high wind and earthquake excitations). However, the large energy consumption required during those extreme events has result in development of semi-active control systems. This type of device cannot exert a force into the structure, but their properties can be adapted practically in real time with only a small delay. Instead of using large amounts of energy, these devices can work with only a battery. This is an important issue because dampers must work under extreme conditions when power outages may occur. Among the multiple existing semi-active devices, this thesis covers three of them: Variable-Orifice Dampers, Magnetorheological dampers and modified friction devices.

#### 3.2. VARIABLE-ORIFICE DAMPER (VOD)

This technology is one of the simplest used for semi-active control. It consists in a conventional viscous damper that has installed an additional valve (mechanically controlled) that can vary the resistance to flow for the fluid within the viscous damper (B.F. Spencer 1999). As a result viscous damping coefficient can range from a lower value (valve 100% opened) to a higher value (valve completely closed) depending on the force required to mitigate vibrations. Fig. 8 shows the conceptualization of the device.

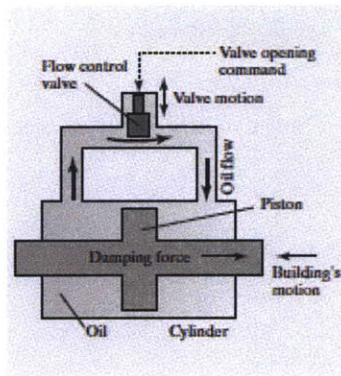


Fig. 8. VOD conceptual model extracted from (Connor 2002).

### 3.3. MAGNETORHEOLOGICAL DAMPERS (MR DAMPERS)

Among this kind of systems, MR Dampers (controllable fluid dampers) are described in this thesis. MR fluids have the special characteristic that under certain magnetic field, they are able to change from free-flowing, linear viscous fluids to semi-solids with controllable yield strength.

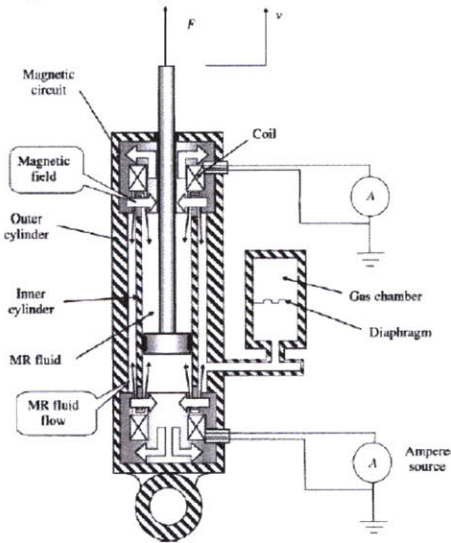


Fig. 9 Scheme for a MR damper (Choi 2001)

Regarding conceptual model, MR is made of a combination of springs, dashpots and a hysteretic device system Fig. 10.

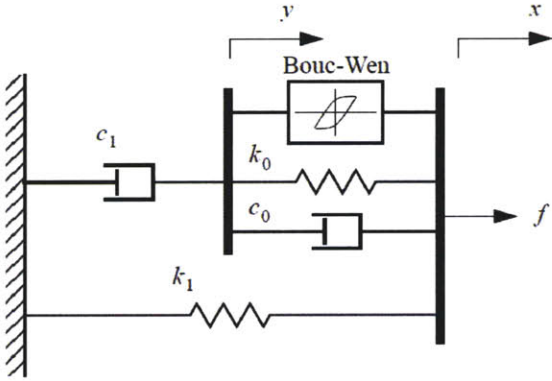


Fig. 10 MR damper and diagonal framing conceptualization

In order to show the change in behavior depending on the voltage applied. A sinusoidal load has been applied on the MR model developed in the thesis (Larrecq 2010). Results are presented in Fig. 11.

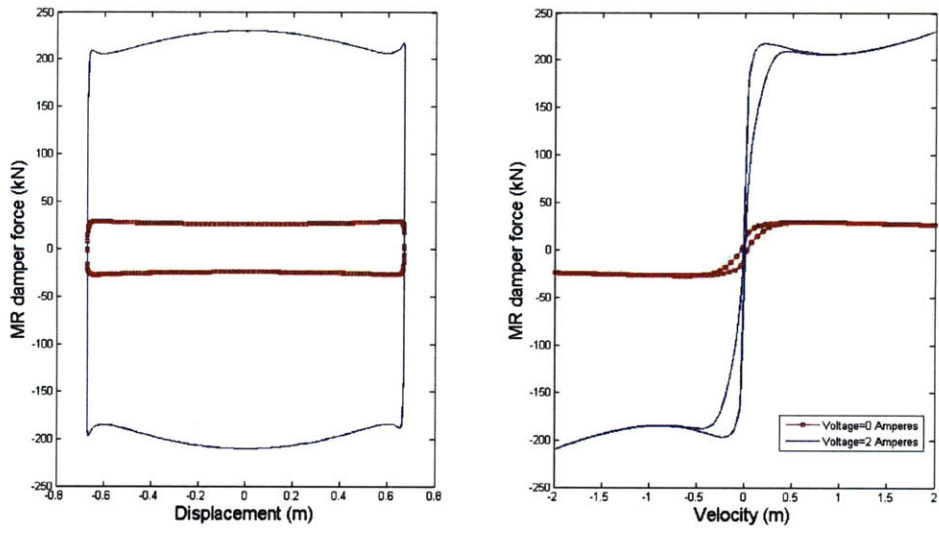


Fig. 11 MR Damper response under sinusoidal loading (Larrecq 2010)



### 3.4. MODIFIED FRICTION DEVICE (MFD)

Another type of device, MFD (controllable friction brake), is presented in this thesis. MFD consists of one drum. Inside this drum, a hydraulic actuator exerts a force on two shoes designed for this purpose. This results in friction when rotation happens. The capability of changing the normal force exerted on the drum involves changes in the friction characteristics as desired. This makes MFD a really interesting device to consider.

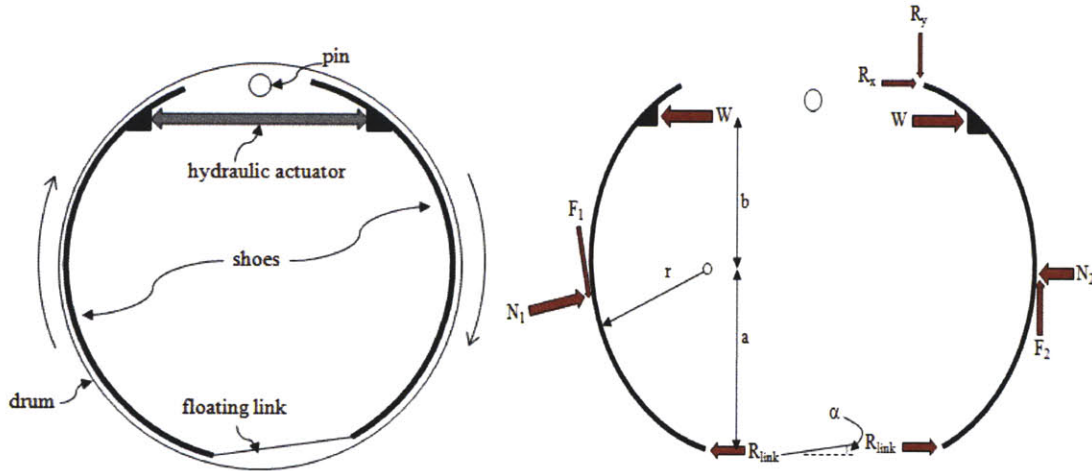
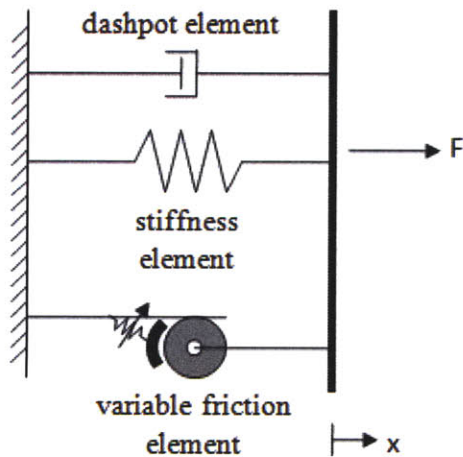


Fig. 12 MFD Duo-Servo drum brake scheme (Laflamme 2010)

The scope of the thesis is to get an economical evaluation of the cost of implementing MFD technology in a 39-story building to compare against the estimated cost of the classical viscous damper implementation.



Regarding conceptual model, MFD is made of a combination of springs, dashpots and a friction device system (Fig. 13).

In order to show the change in behavior depending on the voltage applied (0-12 volts). A sinusoidal load has been applied on the MFD model developed for this purpose (Abdellaoui 2010). Results are presented in Fig. 14.

Fig. 13 MFD conceptualization (Laflamme 2010)

The total force exerted by the MFD is a combination of friction, spring and dashpot forces. Expression for this total force is presented in the next formula (3.1.):

$$F = F_{friction} + k_{mfd} * x + c_{mfd} * \dot{x}^\beta \quad (3.1.)$$

It is really important to consider for this device the temperature increase due to heat generated by friction between surfaces. In order to solve this problem, the device proposed in (Laflamme 2010) mixes steel fiber lining with 15% weight ceramic fibers.

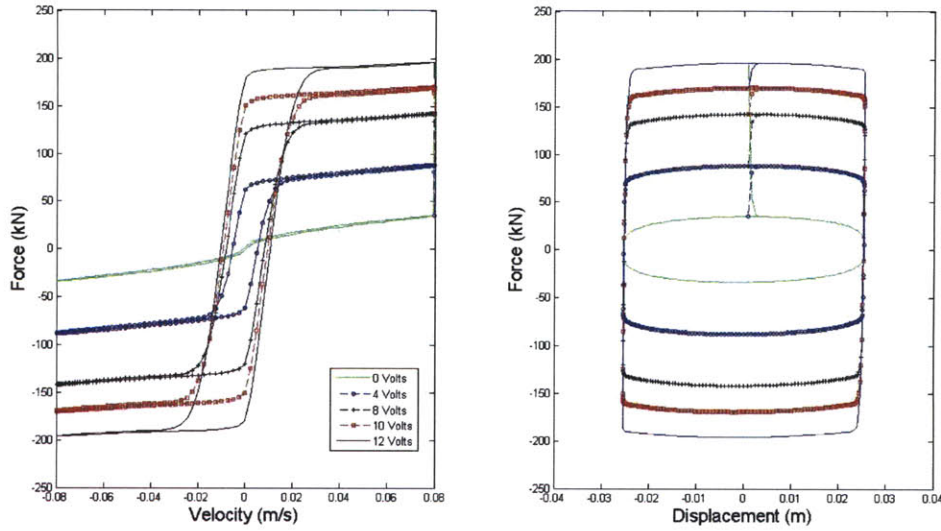


Fig. 14 MFD damper response under sinusoidal loading (Abdellaoui 2010)

Previously, the study has covered the change in behavior of semi-active devices depending on the variable valve opening or variable voltage. However, how these conditions are varied has a big effect on the device's general behavior. Controllers are in charge of deciding the required action based on observations of the structure. The following chapter discusses the most common controllers.

## 4. CONTROL RULES FOR SEMI-ACTIVE DEVICES

### 4.1. INTRODUCTION

Control rules are very important when dealing with active and semi-active devices. These rules are always based on the observations of the system state. Once the observations are measured, the controller decides the action to take and it sends this information to the actuator that acts in consequence to this.

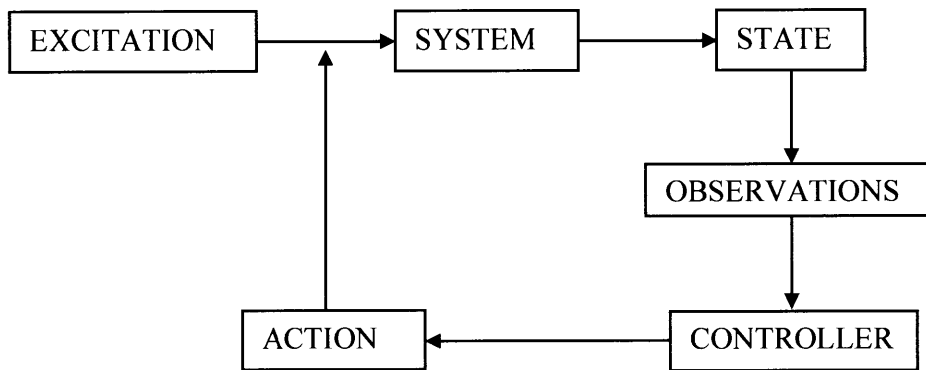


Fig. 15. Flowchart for a controlled system

Regarding structures, based on the observations of the system, optimum force required by the actuator to reduce state in step  $i+1$  is obtained.

Among the multiple optimum force methods, most widely used are: LQR (Linear Quadratic Regulator), H-infinity, and LQG (Linear Quadratic Gaussian). LQR will be discussed in this thesis.

When dealing with active controllers, force required can be directly exerted in the structure (action). However, semi-active devices change properties based on changes in the dynamics of the device (electric field, electromagnetic field or valve orifice) but they cannot exert a force into the structure (they generate a reacting force based on the state of the structure but they can actively change their own dynamics). Hence, the action involves a voltage or valve opening selection. The clipped optimal rule and sliding mode controllers are two controllers discussed in this thesis.

## 4.2. LINEAR QUADRATIC REGULATOR (LQR)

Linear Quadratic Regulator (LQR) optimization is chosen to calculate the force required by the damper. The final aim is to obtain a scalar performance index called  $J$ . As a result of minimizing  $J$ , gain matrix ( $K_f$ ) is obtained. This matrix multiplied by the state vector  $\underline{X}_i$  (containing displacements and velocities for every degree of freedom for step  $i$  provides the force required by the actuators to minimize the damped response state for step  $i+1$ .

$$J = \sqrt{\underline{X}^T * \tilde{Q} * \underline{X} + \underline{u}^T * \tilde{R} * \underline{u}} \quad (4.1.)$$

Q and R are the weight matrices on the state vector ( $\underline{X}$ ) and the damper forces ( $\underline{u}$ ), respectively. There is no method to obtain optimal values for both control matrices. Following heuristic methods, different weight matrices have to be tested until get the desired performance in the system.

### 4.2.1. CLIPPED OPTIMAL RULE

Voltage change leads into an important variation in the general damper efficiency. Hence, the control rule, that is going to be implemented in the system, will play a crucial role in the behavior of the damper. Clipped control rule is implemented at the beginning of the research. Its simplicity and high efficiency make this control rule perfect for these first stages.

Involving this clipped rule, optimum force required by the device is used to decide the voltage to apply to the semi-active system.

Once the force required is known, it is compared to the force exerted by the damper at step  $i$ . If the force generated by the damper for step  $i$  is bigger than the required force, voltage is turned off (0 volts). However, if the force generated by the damper is smaller than the required and the sign of the force is the same than the sign for the velocity of the system, the order is turn on the voltage (12 volts).

Fig. 16 shows the decision scheme for the clipped rule control used in the first stage of the research. The black area corresponds to maximum voltage while the white corresponds to 0 volts.

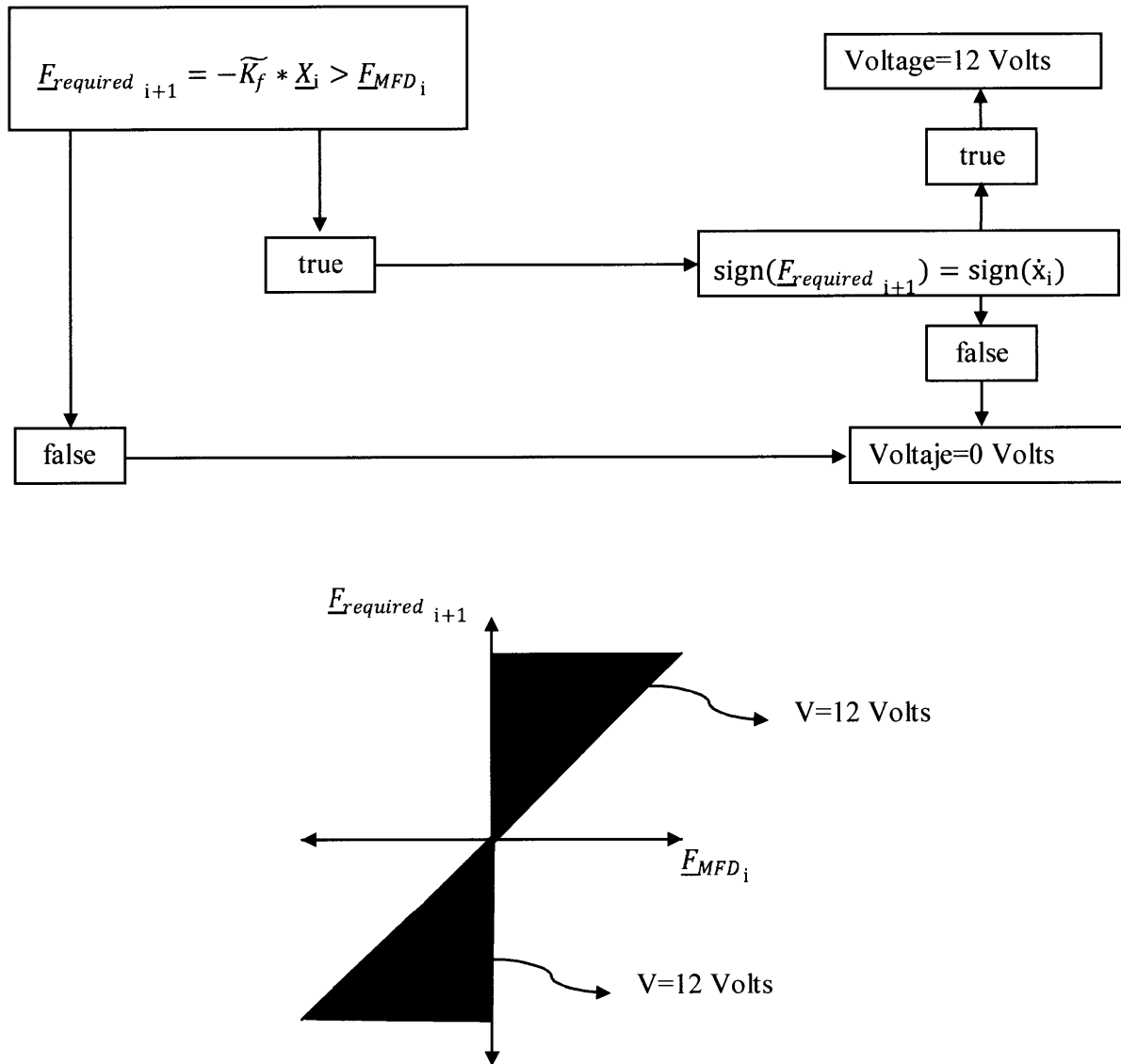


Fig. 16 Clipped rule decision scheme

### 4.3. SLIDING MODE CONTROLLER (LYAPUNOV)

This controller tries to increase the frequency of voltage change in the system in order to increase the efficiency of the device under any circumstance (Laflamme 2010).

This controller is used to control the MFD out of the hysteresis area (velocity close to zero). The final aim is to generate the force required by the LQR. Error is defined as  $e = F_{act} - F_{req}$ . Ideally, this error would tend to zero. However, the device does not have enough capacity to generate the  $F_{req}$  for every state. Hence, voltage is selected in order to minimize this error as much as possible.

Using the squared standard deviation and deriving it, it is obtained the minimum for this function.

$$V = \frac{1}{2} e^2 \quad (4.2.)$$

$$\dot{V} = e \cdot \dot{e} \quad (4.3.)$$

$$\dot{V} = e[\dot{F}_{act} - \dot{F}_{req}] \quad (4.4.)$$

In (Laflamme 2010) it is said that to ensure the negative definiteness of the Lyapunov function (4.2.), the control voltage can be chosen such that:

$$V_{req} = V_{act} + \frac{(-\sigma_2 \ddot{x} - k_{mfd} \dot{x} - \beta c_{mfd} \dot{x}^{\beta-1} + \dot{F}_{req} - \varepsilon e)}{\eta F_{c,0}} \text{sign}(\dot{x}) \quad (4.5.)$$

where  $X$ ,  $\dot{X}$  and  $\ddot{X}$  represent the state of the system.  $\varepsilon$  represents the system uncertainty and  $\eta$  represents the delay of the voltage. The other factors in the equation are intrinsic to the MFD nature. To get the complete mathematical basis for this control method, consult (Laflamme 2010).

## 5. MODEL VERIFICATION

### 5.1. MASS AND STIFFNESS MATRIX EXTRACTION METHODOLOGY

The SAP2000 structural model is used as a base for the structure stiffness and mass extraction. First, ultra-stiff elements are added to the model to lump the behavior of every floor in a single 3 degree of freedom (DOF) element which is going to contain the stiffness in the X and Y direction plus rotation in Z axis (torsion). Furthermore, the mass of the whole story is lumped at those points. Known that the ultra-stiff additional elements are going to introduce unrealistic stiffness in the model, the final stiffness matrix (K) obtained is proportionally scaled to obtain the dynamic and static behavior of the initial model (deflection subjected to static loading, periods of vibration and mass participation factors).

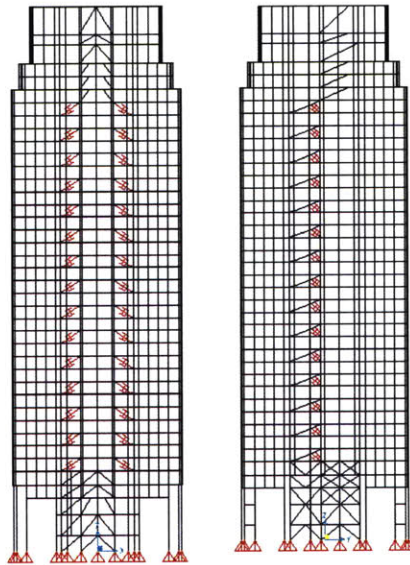


Fig. 17. SAP2000 structural model for the X and Y directions

The methodology used to extract the stiffness matrix consisted in restraining interstory movements and rotations. Afterwards, unitary displacement at the top of each floor, for every desired direction (X, Y and Z rotation), is applied. As a result, the reactions obtained in the floor are equal to the stiffness of this floor in the direction where the displacement is applied (Fig. 18).

$$F = K * x \rightarrow x = 1 \rightarrow F = K \quad (5.1.)$$

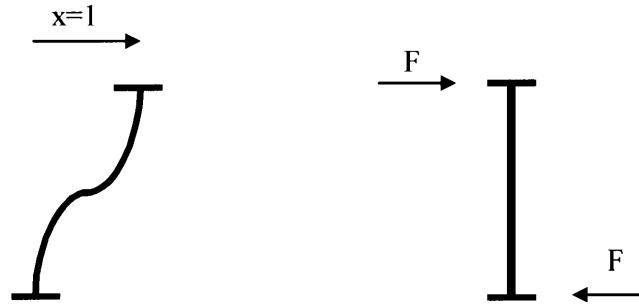


Fig. 18. Stiffness extraction from a 3D frame model for the X direction

In the paper developed by (R. a. McNamara 2003), 1% proportional damping was chosen for the building undergoing seismic excitation. In this thesis, 5.26 and 5 seconds have been chosen calculate the Rayleigh proportional damping (matching the first two periods of vibration for the structure). This results in coupled (complex) eigenvalues for the structure.

## 5.2. MODAL ANALYSIS COMPARISON

As described in the previous chapter, K matrix was scaled in such a way that the static deflection was similar to the one obtained for the initial structural model. After this step, first 6 periods of vibration and mass participation factor were extracted, yielding the following results. Final stiffness, mass and damping matrix are presented in Appendix B (building structural properties).

Mode Shape	1	2	3	4	5	6
Period (sec)	5.26	5.00	3.65	1.92	1.82	1.71
Effective Mass (%)	66.1	62.6	81.2	15.3	12.8	8.5
Direction	X (E-W)	Y (N-S)	Rotation	X (E-W)	Y (N-S)	Rotation

Table 2. Data extracted from (R. a. McNamara 2003)



Mode Shape	1	2	3	4	5	6
Period (sec)	5.27	4.97	3.63	2.15	2.05	1.73
Effective Mass (%)	65.62	63.69	66.04	15.15	14.77	25.85
Direction	X (E-W)	Y (N-S)	Rotation	X (E-W)	Y (N-S)	Rotation

Table 3. Data obtained from the lumped model

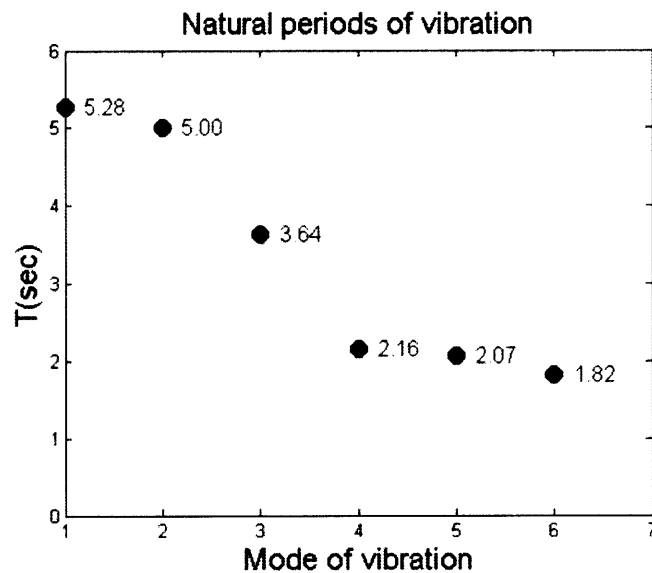


Fig. 19. Periods of vibration for the lumped model

### 5.3. LOAD CASES

#### 5.3.1. WIND LOAD

Regarding wind loads, just time history acceleration at the roof is available in the literature. Because of this, loading cannot be extrapolated to generate the same simulation. Data available from another similar structure (Fig. 20) has been used. The peak wind load is scaled in such a way that the same peak acceleration will be generated on the 37<sup>th</sup> floor, as the one provided in the literature (R. a. McNamara 2003).

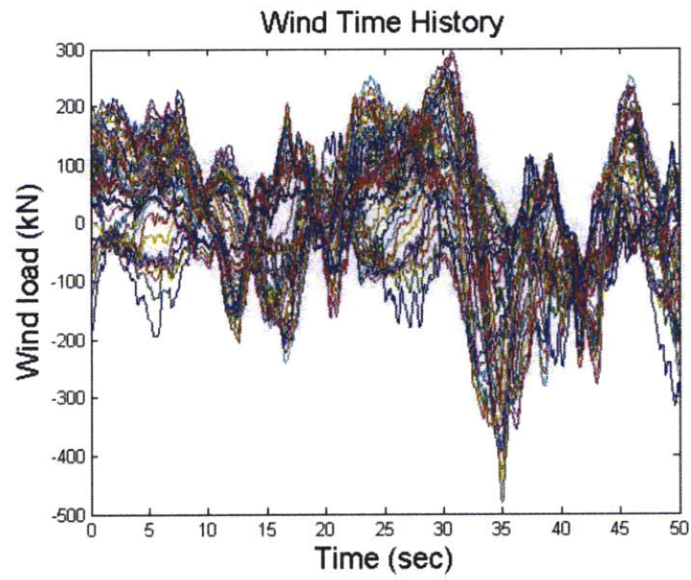


Fig. 20 Wind load time history

#### 5.4. RESULTS

		Wind tunnel results	Lumped model	Lumped model	Wind tunnel results
		E-W (X) Dir.	E-W (X) Dir.	N-S (Y) Dir.	N-S (Y) Dir
Response without dampers	accel. at 37 <sup>th</sup> Flr.(m/s <sup>2</sup> )	0.70	0.64	0.45	0.41
	displ. at 37 <sup>th</sup> Flr.(m/s)	0.53	0.40	0.28	0.28
	Base Shear (kN)	17378	9267	12913	6140
Response with dampers	accel. at 37 <sup>th</sup> Flr.(m/s <sup>2</sup> )	0.52	0.42	0.30	0.32
	displ. at 37 <sup>th</sup> Flr.(m/s)	0.42	0.30	0.19	0.25
	Base Shear (kN)	14109	5871	9065	5163

Table 4. Data extracted from (R. a. McNamara 2003) and data obtained from the lumped model

## 6. SIMULATIONS

### 6.1. GENERAL STRATEGY

The  $n$  degrees of freedom model's behavior is simulated in MATLAB. Among the different state space formulations available, Direct Integration is used in this thesis. The formulation for this method is presented in equations 6.1, 6.2 and 6.3.

$$\bar{\dot{X}}_t = \begin{bmatrix} \dot{X}_1 \\ \dot{X}_2 \\ \vdots \\ \dot{X}_i \\ \vdots \\ \dot{X}_n \\ \frac{\dot{X}_1}{X_1} \\ \dot{X}_2 \\ \vdots \\ \dot{X}_i \\ \vdots \\ \dot{X}_n \end{bmatrix}_t \quad \bar{X}_t = \begin{bmatrix} X_1 \\ X_2 \\ \vdots \\ X_i \\ \vdots \\ X_n \\ \frac{X_1}{X_1} \\ X_2 \\ \vdots \\ X_i \\ \vdots \\ X_n \end{bmatrix}_t \quad \tilde{A}p = \begin{bmatrix} \Omega & I \\ -\tilde{M}^{-1} * \tilde{K} & -\tilde{M}^{-1} * \tilde{C} \end{bmatrix} \quad (6.1)$$

$$\bar{X}_{t+1} = e^{\tilde{A}p * \Delta t} * \bar{X}_t + \tilde{A}p^{-1} * (e^{\tilde{A}p * \Delta t} - \tilde{I}) \left( \begin{bmatrix} \Omega \\ -\tilde{M}^{-1} * \bar{B}_w \end{bmatrix} * \bar{w}_t + \begin{bmatrix} \Omega \\ -\tilde{M}^{-1} * \bar{B}_f \end{bmatrix} * \bar{u}_t \right) \quad (6.2)$$

$$\bar{X}_{t+1} = \tilde{A}p * \bar{X}_{t+1} + \begin{bmatrix} \Omega \\ -\tilde{M}^{-1} * \bar{B}_w \end{bmatrix} * \bar{w}_t + \begin{bmatrix} \Omega \\ -\tilde{M}^{-1} * \bar{B}_f \end{bmatrix} * \bar{u}_t \quad (6.3)$$

In the previous equations,  $\tilde{M}$  is the matrix containing the mass of the building for every degree of freedom,  $\tilde{K}$  is the stiffness matrix and  $\tilde{C}$  is the damping matrix.  $\bar{X}_{t+1}$  is a vector that contains all the displacements and velocities of the system at step  $t+1$  and  $\bar{\dot{X}}_{t+1}$  contains all the velocities and accelerations of the system at step  $t+1$ .  $\tilde{I}$  is the identity matrix.  $\bar{B}_w$  is a vector with  $2n$  elements (zeros for the first  $n$  elements and ones for the latter  $n$  elements),  $\bar{w}_t$  is a vector with zeros for the first  $n$  elements and in the last  $n$  elements

wind loading is stored at time step  $t+1$ .  $\bar{B}_f$  is a matrix with  $2n \times m$  elements ( $m$  is the number of actuators throughout the building and  $n$  is the number of degrees of freedom) whose bottom half contains the location of the devices.  $\bar{u}_t$  is very similar to  $\bar{w}_t$ , but the second half contains the forces exerted by either the viscous dampers or the MFDs.

Once the model developed is proved to be accurate enough to model the general behavior of a 39-story building, MFDs are incorporated to obtain a similar performance to the one achieved by viscous dampers.

The chosen time delay in the signal to the semi-active device is one time step ( $\Delta t = 0.005\text{sec}$ ). Regarding weight matrices (Q and R), there is no method to obtain optimal values for both control matrices. The values for Q and R are chosen in order prevent the MFD from working at full voltage out of the hysteresis area (displacements close to zero). The main reason is that this would increase accelerations in the building while the target of this study is to reduce them.

First, MFDs are placed in the same locations than the initial viscous dampers (every 2 stories). Next, additional layouts using devices every 4, 6 and 8 stories with increasing MFD capacity (600 kN, 1000 kN and 2000 kN respectively) are simulated. Every scheme is studied under wind loading conditions to evaluate the performance of both devices when trying to reduce accelerations in the building.

After these initial simulations, a new strategy based on energy dissipated (6.4) by every device is developed. Devices with smaller participation in correcting building state (less energy dissipated) are removed from the design. Analysis is rerun in order to compare the efficiency of every scheme until an optimum distribution is obtained.

$$E_j = \sum_{t=1}^{t=steps} u_{t,j} * ((x_{t,j+1} - x_{t,j}) - (x_{t-1,j+1} - x_{t-1,j})) \quad j=1,2,\dots,m \quad (6.4)$$

where  $u_{t,j}$  is the force exerted at step  $t$  by the device between story  $j$ th and  $j+1$ th.  $x_{t,j+1}$  is displacement at step  $t$  for story  $j+1$ .  $m$  is the number of actuators considered in the simulation.

## 6.2. MFD 200 kN EVERY 2 STORIES

		Wind Load Case	
		E-W (X) Dir.	N-S (Y) Dir.
Response without dampers	accel. at 37 <sup>th</sup> Flr.(m/s <sup>2</sup> )	0.64	0.41
	displ. at 37 <sup>th</sup> Flr.(m/s)	0.40	0.28
	Base Shear (kN)	9267	6140
Response with MFD	accel. at 37 <sup>th</sup> Flr.(m/s <sup>2</sup> )	0.46	0.36
	displ. at 37 <sup>th</sup> Flr.(m/s)	0.30	0.24
	Base Shear (kN)	6284	5058

Table 5. Data obtained from the lumped model

Floor	Work X direction (kN*m)	Work Y direction (kN*m)
5	29.2	24.6
7	35.8	20.2
9	25.3	20.3
11	41.2	29.0
13	40.9	28.9
15	44.2	33.0
17	44.0	32.2
19	48.9	38.3
21	47.1	35.2
23	55.5	45.1
25	52.6	40.7
27	54.0	41.7
29	46.2	34.8
31	40.1	32.9
33	28.6	22.7

Table 6. Work done by the MFD's

Floor	Work X direction (kN*m)	Work Y direction (kN*m)
5	27.7	18.5
7	32.3	19.0
9	31.5	18.8
11	46.6	27.8
13	45.8	27.6
15	52.8	31.9
17	50.0	30.9
19	59.8	38.0
21	54.1	34.2
23	72.2	47.9
25	62.6	42.9
27	46.2	24.0
29	37.6	19.8
31	34.0	19.4
33	22.1	13.4

Table 7. Work done by viscous damper scheme

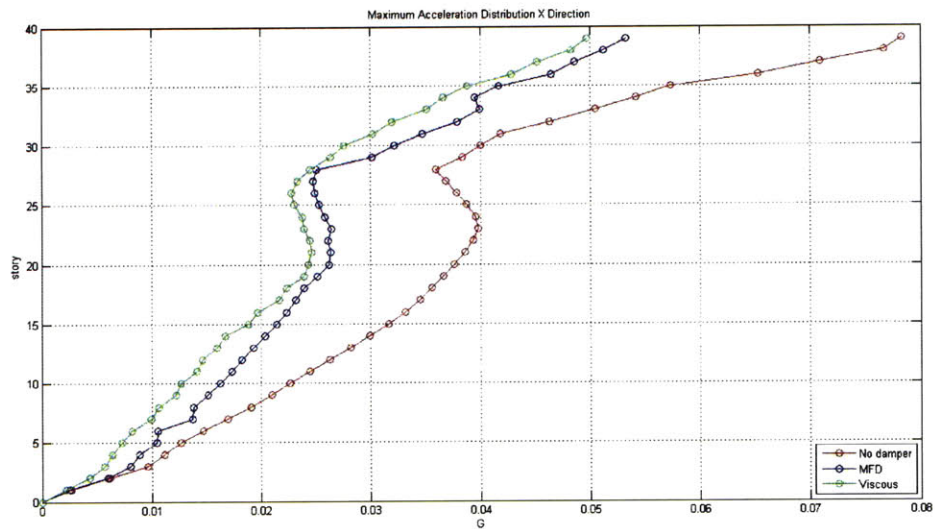


Fig. 21 Maximum acceleration profile for X direction

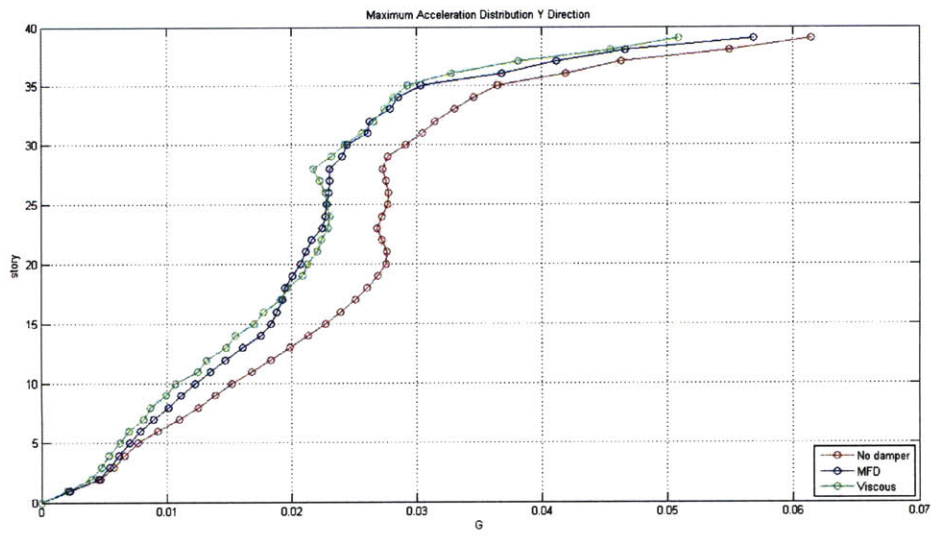


Fig. 22 Maximum acceleration profile for Y direction

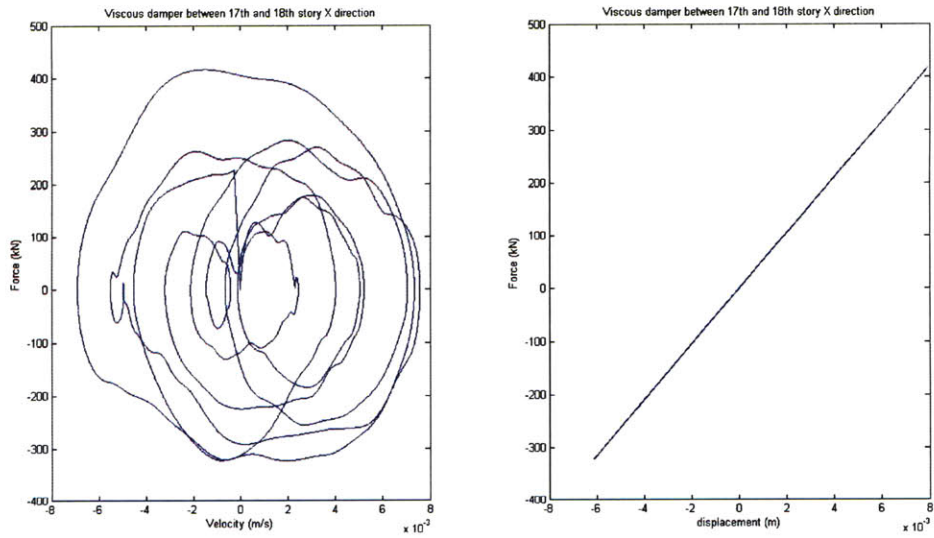


Fig. 23 Viscous damper behavior between 17<sup>th</sup> and 18<sup>th</sup> floor for X Direction

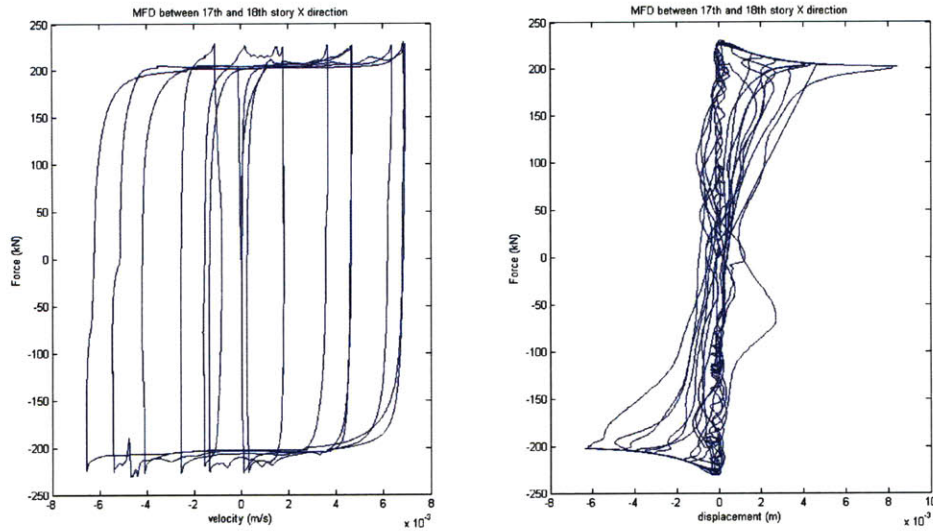


Fig. 24 MFD behavior between 17<sup>th</sup> and 18<sup>th</sup> floor X Direction

It is important to compare the maximum capacity for both devices. The viscous damper is exerting a maximum force of 400 kN (Fig. 23), while the MFD maximum capacity is half of this (Fig. 24). See in Fig. 21 and Fig. 22 that acceleration reduction is similar for both cases, but because of the control designed for the semi-active devices, much better efficiency in terms of maximum capacity of the device is obtained.

### 6.3. HEURISTIC STRATEGY

The way to remove devices for this first strategy consists in maintaining the spacing between MFDs. After checking the 2 floor spacing semi-active scheme behavior in section 6.2, devices are removed keeping a device spacing of 4, 6 and 8 stories. After every step, MFD maximum capacity is increased until behavior of the structure is similar to the viscous damper design. In addition to the increase of the device's maximum capacity, Q and R weight matrices are adapted to prevent MFDs working at full voltage (maximum friction) out of the hysteretic region (displacements close to zero). The reason to adapt MFDs behavior relies on the increase of accelerations in the system when MFD is working full voltage out of the maximum velocity area (regular friction device behavior).



### 6.3.1. MFD 600 kN EVERY 4 STORIES

		Wind Load Case	
		E-W (X) Dir.	N-S (Y) Dir.
Response without dampers	accel. at 37 <sup>th</sup> Flr.(m/s <sup>2</sup> )	0.64	0.41
	displ. at 37 <sup>th</sup> Flr.(m/s)	0.40	0.28
	Base Shear (kN)	9267	6140
Response with MFD	accel. at 37 <sup>th</sup> Flr.(m/s <sup>2</sup> )	0.43	0.35
	displ. at 37 <sup>th</sup> Flr.(m/s)	0.28	0.24
	Base Shear (kN)	5652	4635

Table 8.Data obtained from the lumped model

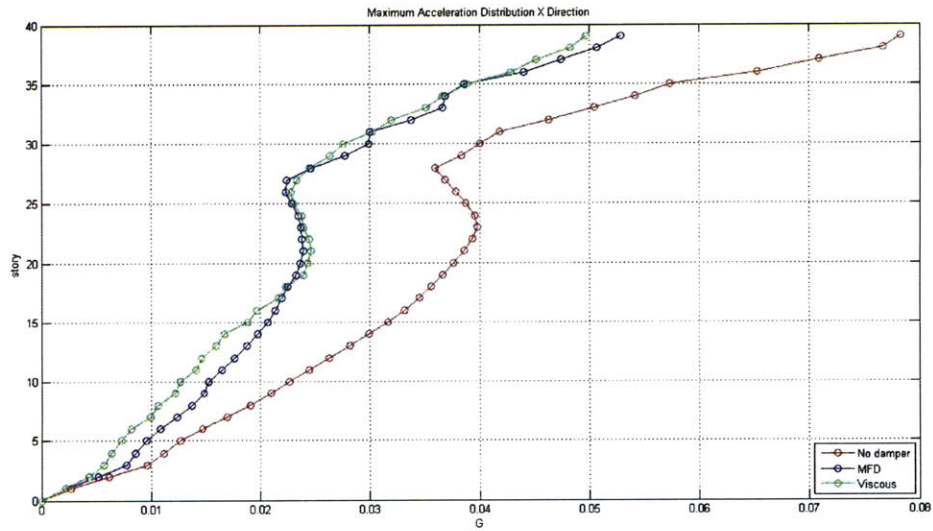


Fig. 25 Maximum acceleration profile for X direction

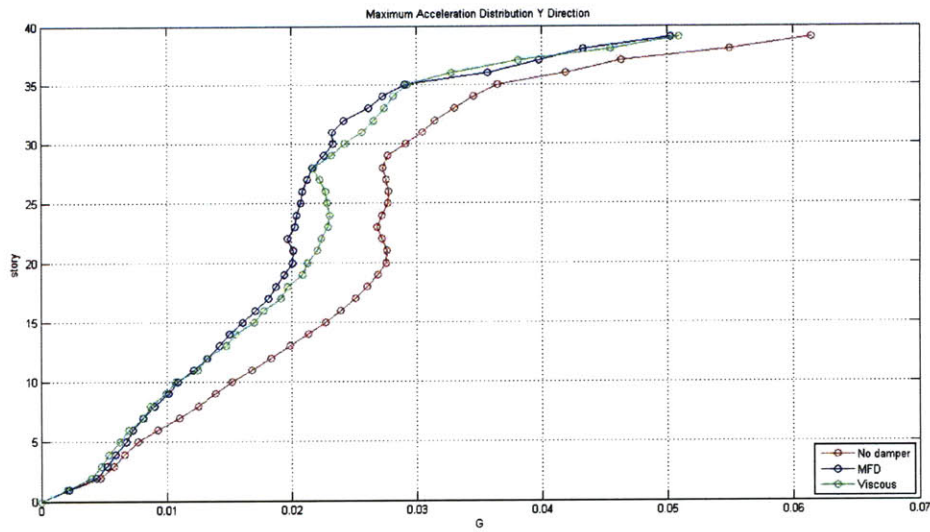


Fig. 26 Maximum acceleration profile for Y direction

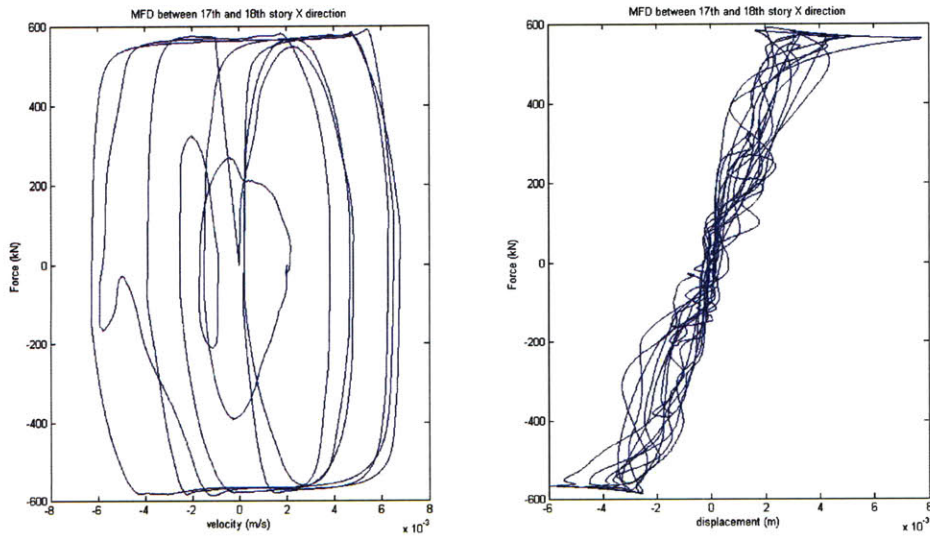


Fig. 27 MFD behavior between 17<sup>th</sup> and 18<sup>th</sup> floor X Direction

Acceleration reduction for this first iteration is better than the reduction obtained for the viscous damper scheme (Fig. 25 and Fig. 26). The maximum capacity of the MFD is increased to 600 kN. In Fig. 27, velocity against MFD force is displayed on the left part. The controller shows a smooth behavior in the area of maximum velocities that prevents the device from generating high accelerations when the sign of the velocity changes (non-modified friction device).

### 6.3.2. MFD 1000 kN EVERY 6 STORIES

		Wind Load Case	
		E-W (X) Dir.	N-S (Y) Dir.
Response without dampers	accel. at 37 <sup>th</sup> Flr.(m/s <sup>2</sup> )	0.64	0.41
	displ. at 37 <sup>th</sup> Flr.(m/s)	0.40	0.28
	Base Shear (kN)	9267	6140
Response with MFD	accel. at 37 <sup>th</sup> Flr.(m/s <sup>2</sup> )	0.43	0.33
	displ. at 37 <sup>th</sup> Flr.(m/s)	0.28	0.24
	Base Shear (kN)	5644	4584

Table 9. Data obtained from the lumped model

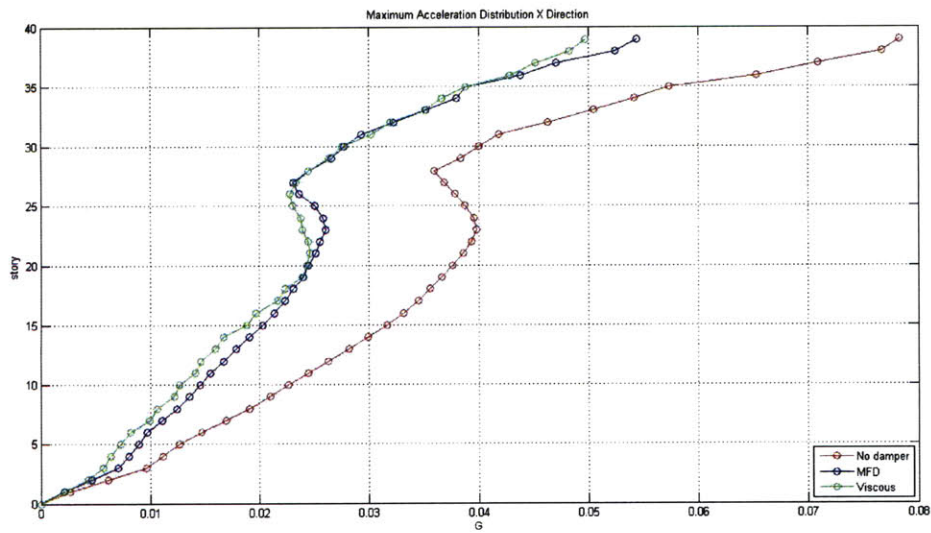


Fig. 28 Maximum acceleration profile for X direction

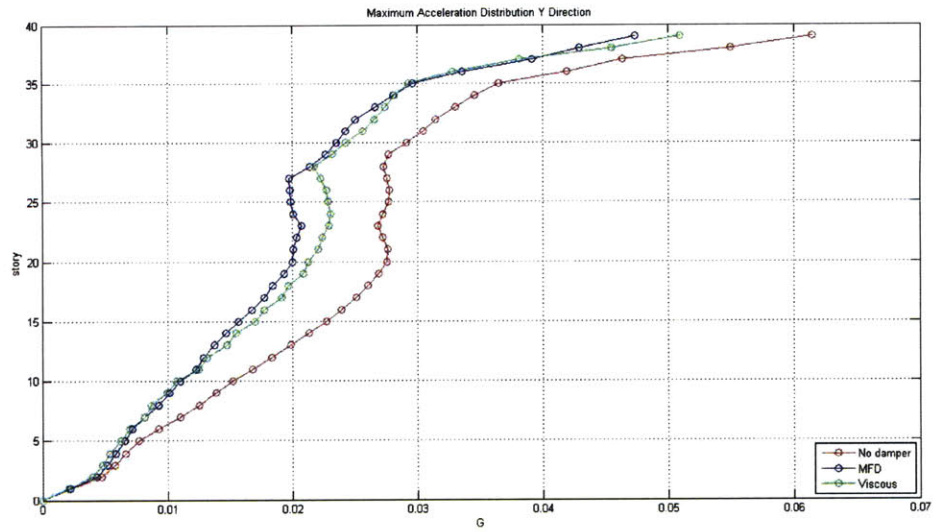


Fig. 29 Data Maximum acceleration profile for Y direction

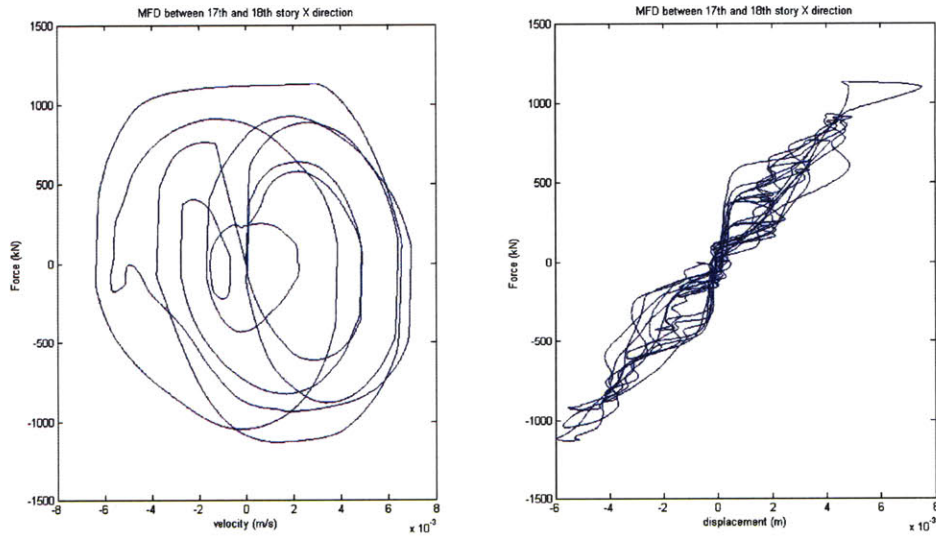


Fig. 30 MFD behavior between 17<sup>th</sup> and 18<sup>th</sup> floor X Direction

Similar conclusions than those stated in section 6.3.1 could be provided for this iteration. However, there is an important difference to point out. Fig. 30 shows the behavior of the MFD between floors 17<sup>th</sup> and 18<sup>th</sup> for the X direction, the controller is be relaxed to get the acceleration reduction desired, as a result of this, MFD behavior starts to seem like a viscous damper behavior. Hence, MFD starts to be inefficient (it does not work as it should) for this scheme.

### 6.3.3. MFD 2400 kN EVERY 8 STORIES

		Wind Load Case	
		E-W (X) Dir.	N-S (Y) Dir.
Response without dampers	accel. at 37 <sup>th</sup> Flr.(m/s <sup>2</sup> )	0.64	0.41
	displ. at 37 <sup>th</sup> Flr.(m/s)	0.40	0.28
	Base Shear (kN)	9267	6140
Response with MFD	accel. at 37 <sup>th</sup> Flr.(m/s <sup>2</sup> )	0.44	0.36
	displ. at 37 <sup>th</sup> Flr.(m/s)	0.28	0.25
	Base Shear (kN)	5609	4533

Table 10. Data obtained from the lumped model

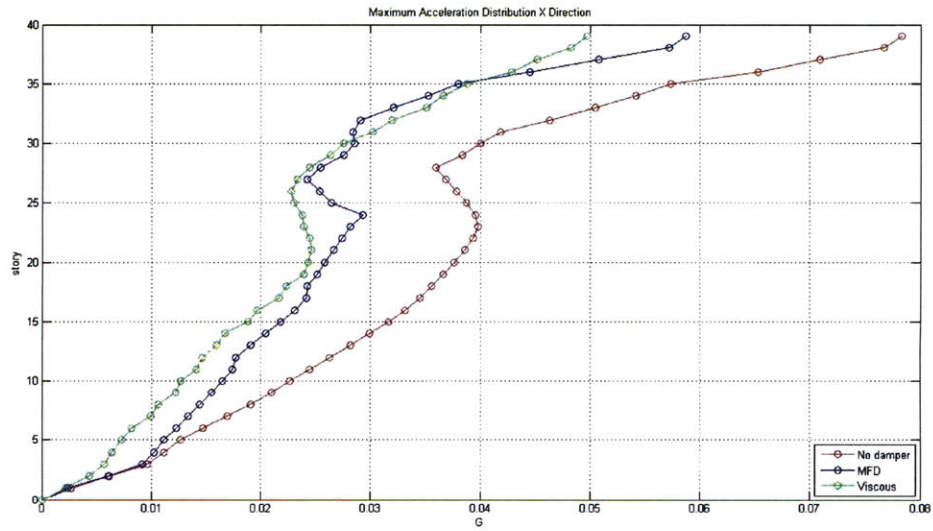


Fig. 31. Maximum acceleration profile for X direction

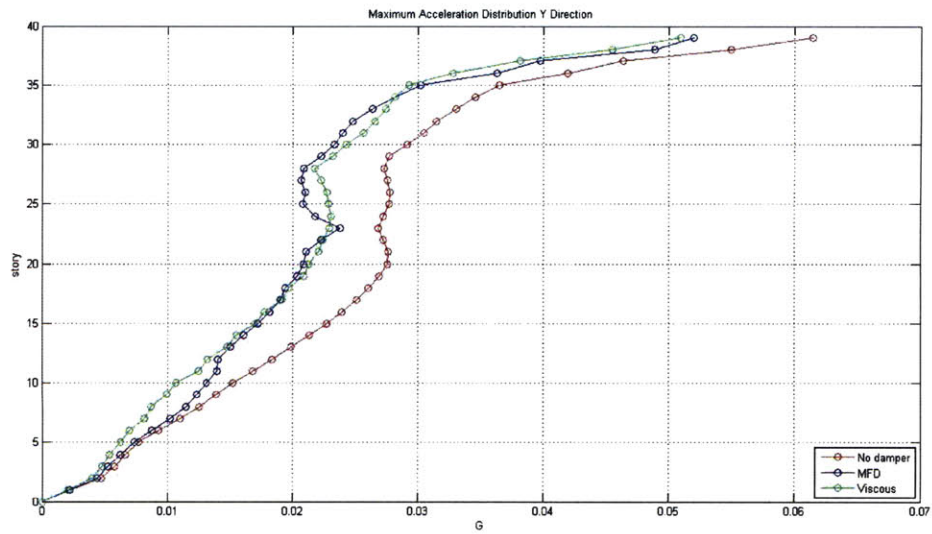


Fig. 32. Data Maximum acceleration profile for Y direction

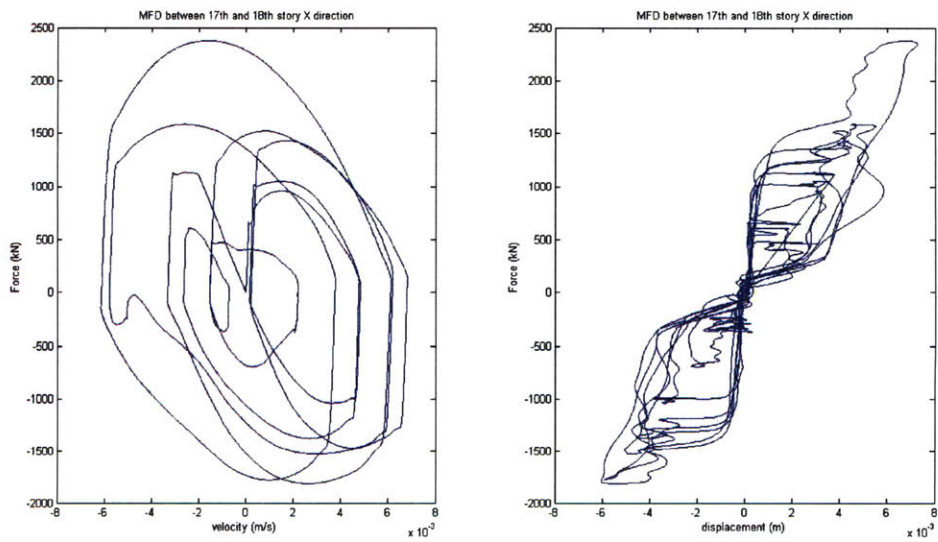


Fig. 33. MFD behavior between 17<sup>th</sup> and 18<sup>th</sup> floor X Direction

Fig. 31 and Fig. 32 show that MFD between story 24<sup>th</sup> and 25<sup>th</sup> is problematic when trying to reduce the accelerations. As a result, control is relaxed for this device in order to smooth the behavior. The same problem than 6.3.2 presented is observed in this iteration. Fig. 33 seems more a viscous behavior than a friction one as a result of the control relaxation.

#### 6.4. STRATEGY BASED ON ENERGY DISSIPATION.

Keeping equal spacing between dampers seems a reasonable strategy. However, wind load is not uniformly distributed throughout the building. As a result, regular spacing may not be efficient in terms of wind excitation reduction. A second strategy is developed to decide which devices are going to be kept and which ones are going to be removed from the building. After analyzing the energy dissipated by every device (work done), those devices exerting smaller work into the structure are going to be removed gradually. At the same time, Q and R matrices are adapted to the new configuration and the device maximum capacity is increased to get similar acceleration reduction than the viscous damper original design.

##### 6.4.1. 1<sup>ST</sup> ITERATION (400 KN MFD)

		Wind Load Case	
		E-W (X) Dir.	N-S (Y) Dir.
Response without dampers	accel. at 37 <sup>th</sup> Flr.(m/s <sup>2</sup> )	0.64	0.41
	displ. at 37 <sup>th</sup> Flr.(m/s)	0.40	0.28
	Base Shear (kN)	9267	6140
Response with MFD	accel. at 37 <sup>th</sup> Flr.(m/s <sup>2</sup> )	0.42	0.35
	displ. at 37 <sup>th</sup> Flr.(m/s)	0.27	0.24
	Base Shear (kN)	5420	4257

Table 11. Data obtained from the lumped model

Floor	Work X direction (kN*m)	Work Y direction (kN*m)
7	46.6	39.1
11	63.2	54.8
13	63.0	54.8
15	70.5	62.0
17	68.6	60.5
19	78.4	71.0
21	73.1	64.5
23	87.9	81.0
25	78.5	72.3
27	79.4	72.7
29	66.2	59.8
31	57.8	55.6

Table 12. Work done by the MFD's

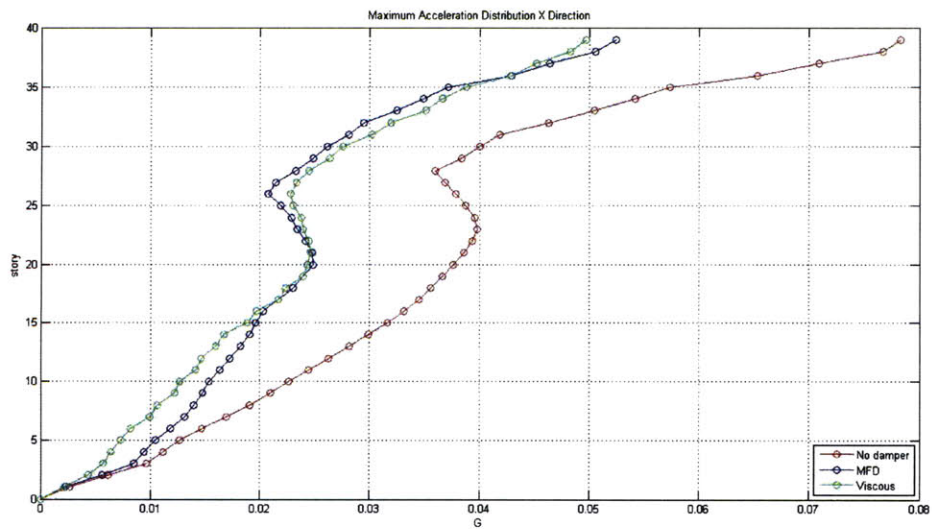


Fig. 34. Maximum acceleration profile for X direction



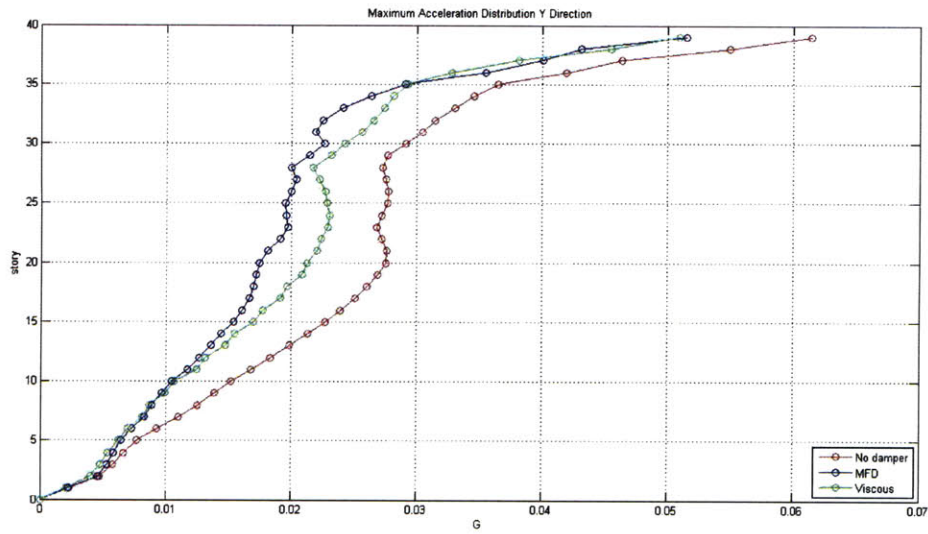


Fig. 35. Data Maximum acceleration profile for Y direction

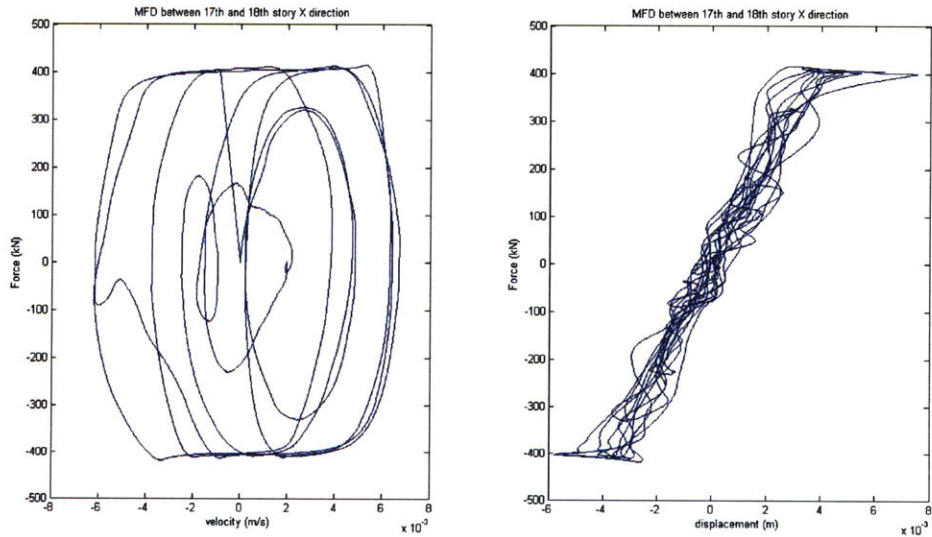


Fig. 36. MFD behavior between 17<sup>th</sup> and 18<sup>th</sup> floor X Direction

In this first iteration, devices in stories 5, 9 and 33 are removed. MFD maximum capacity is 400 kN. The acceleration reduction for both directions is slightly better than the one obtained for viscous dampers (Fig. 34 and Fig. 35). The behavior of one of the devices is presented in Fig. 36. This plot shows a very smooth behavior when velocities are high while maintaining a friction nature when velocities are closer to zero.

6.4.2. 2<sup>ND</sup> ITERATION (400 kN MFD)

		Wind Load Case	
		E-W (X) Dir.	N-S (Y) Dir.
Response without dampers	accel. at 37 <sup>th</sup> Flr.(m/s <sup>2</sup> )	0.64	0.41
	displ. at 37 <sup>th</sup> Flr.(m/s)	0.40	0.28
	Base Shear (kN)	9267	6140
Response with MFD	accel. at 37 <sup>th</sup> Flr.(m/s <sup>2</sup> )	0.44	0.36
	displ. at 37 <sup>th</sup> Flr.(m/s)	0.29	0.24
	Base Shear (kN)	5841	4476

Table 13. Data obtained from the lumped model

Floor	Work X direction (kN*m)	Work Y direction (kN*m)
15	77.1	76.1
17	75.3	74.9
19	85.2	83.7
21	79.7	78.2
23	94.7	91.8
25	85.2	83.6
27	86.1	82.5
29	72.0	68.9
31	63.4	59.5

Table 14. Work done by the MFD's

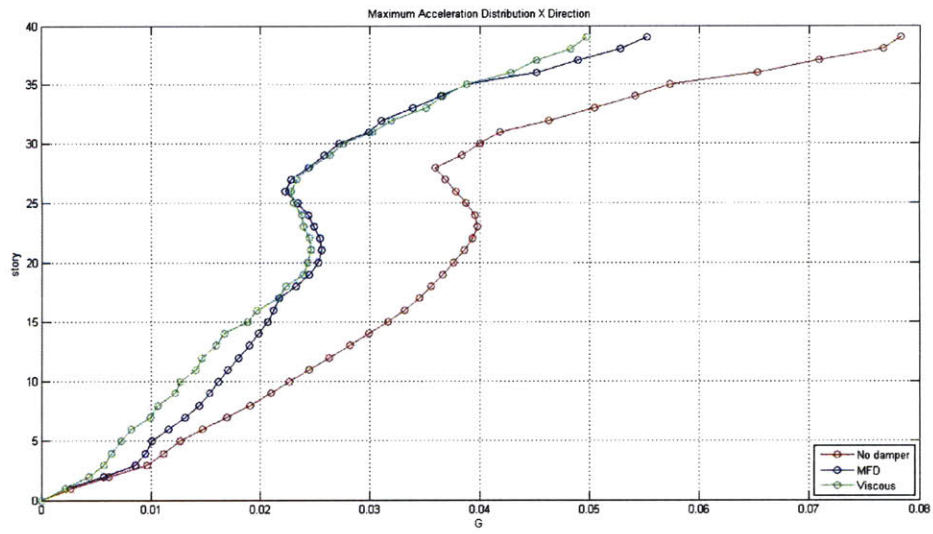


Fig. 37. Data Maximum acceleration profile for X direction

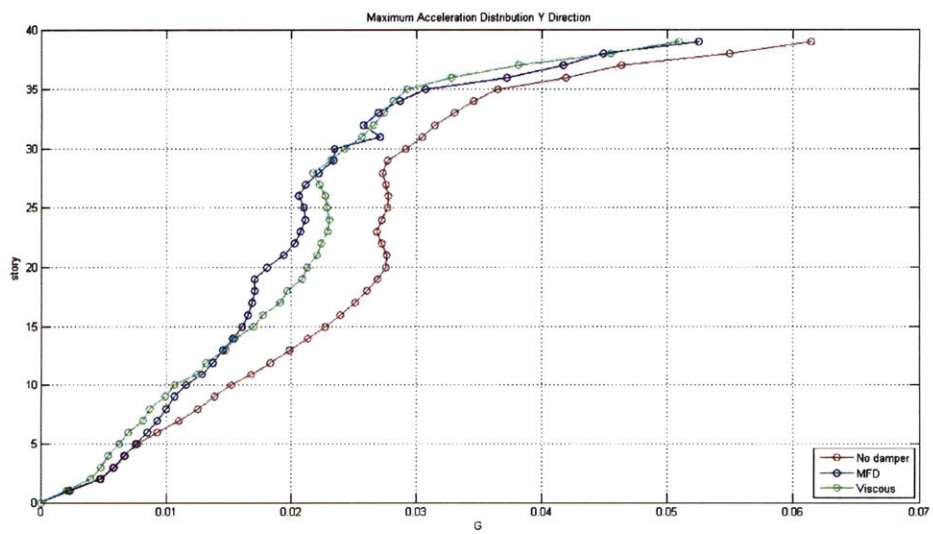


Fig. 38. Data Maximum acceleration profile for Y direction

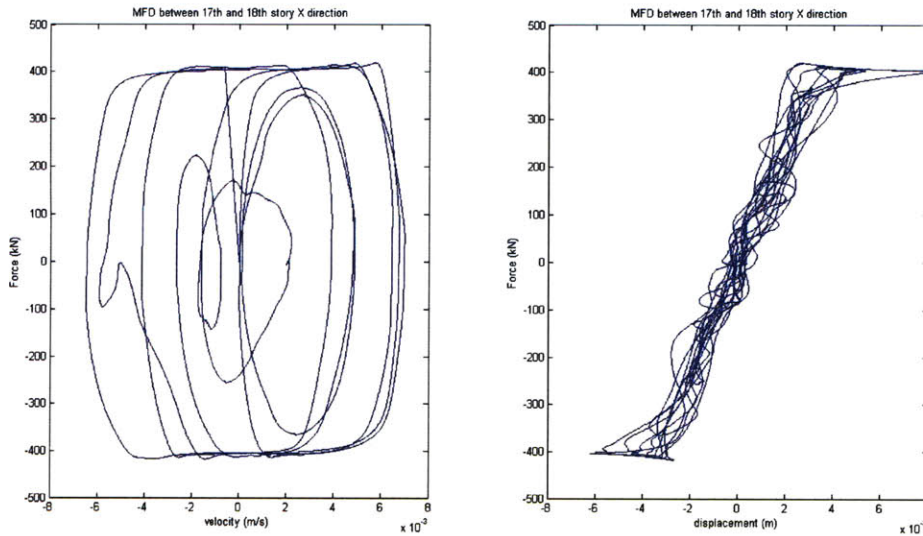


Fig. 39. MFD behavior between 17<sup>th</sup> and 18<sup>th</sup> floor X Direction

Second iteration removes devices in stories 7, 11 and 13. MFD maximum capacity is kept as 400 kN. The acceleration reduction for both directions similar to the one obtained for viscous dampers (Fig. 34 Fig. 37 and Fig. 38). The behavior of one of the devices is presented in Fig. 36.

This behavior shows a very smooth behavior when velocities are high while maintaining a friction nature when velocities are closer to zero. The device in story 31 for the Y direction is critical in the design of this iteration (Fig. 38). The control is relaxed to avoid full voltage in the device when velocities are high.

#### 6.4.3. 3<sup>RD</sup> ITERATION (800 kN MFD)

		Wind Load Case	
		E-W (X) Dir.	N-S (Y) Dir.
Response without dampers	accel. at 37 <sup>th</sup> Flr.(m/s <sup>2</sup> )	0.64	0.41
	displ. at 37 <sup>th</sup> Flr.(m/s)	0.40	0.28
	Base Shear (kN)	9267	6140
Response with MFD	accel. at 37 <sup>th</sup> Flr.(m/s <sup>2</sup> )	0.40	0.35
	displ. at 37 <sup>th</sup> Flr.(m/s)	0.25	0.24
	Base Shear (kN)	5034	4550

Table 15. Data obtained from the lumped model

Floor	Work X direction (kN*m)	Work Y direction (kN*m)
15	139.9	83.5
17	136.9	79.8
19	151.7	96.0
21	142.6	84.6
23	157.6	115.0
25	141.4	101.7
27	136.0	107.3

Table 16. Work done by the MFD's

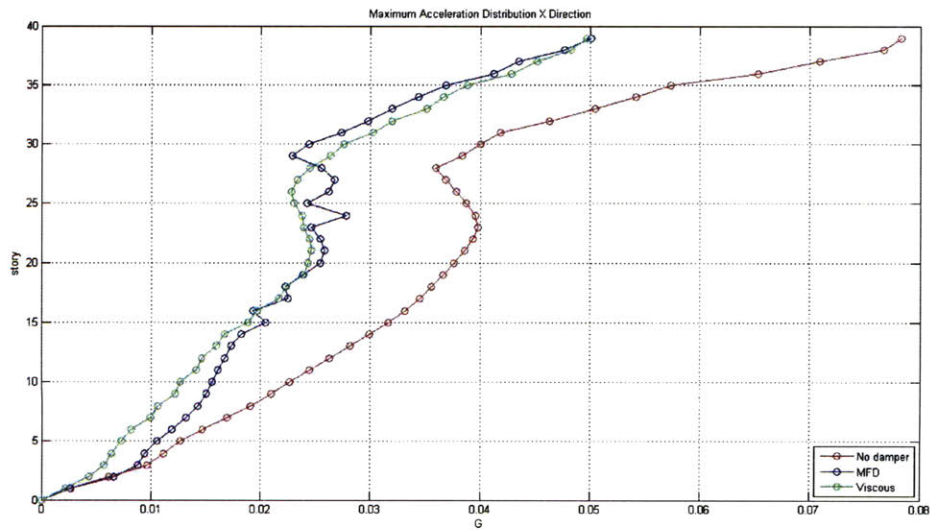


Fig. 40. Data Maximum acceleration profile for X direction

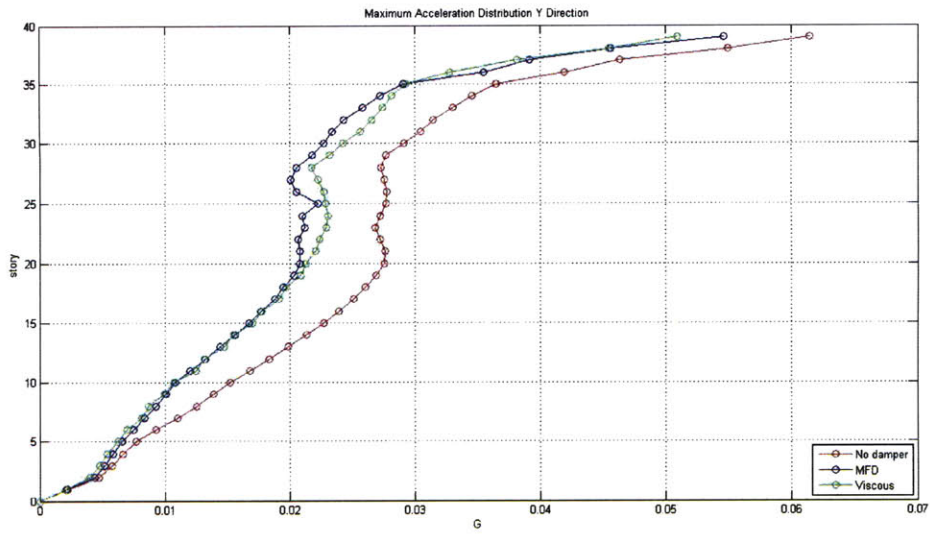


Fig. 41. Data Maximum acceleration profile for Y direction

The third iteration involves removing devices in stories 29 and 31. In the design of the controllers for each device, MFD between floors 24 and 25 is the most critical (Fig. 40 and Fig. 41). Control is relaxed just for this device to generate a smooth behavior which reduces accelerations in the building.

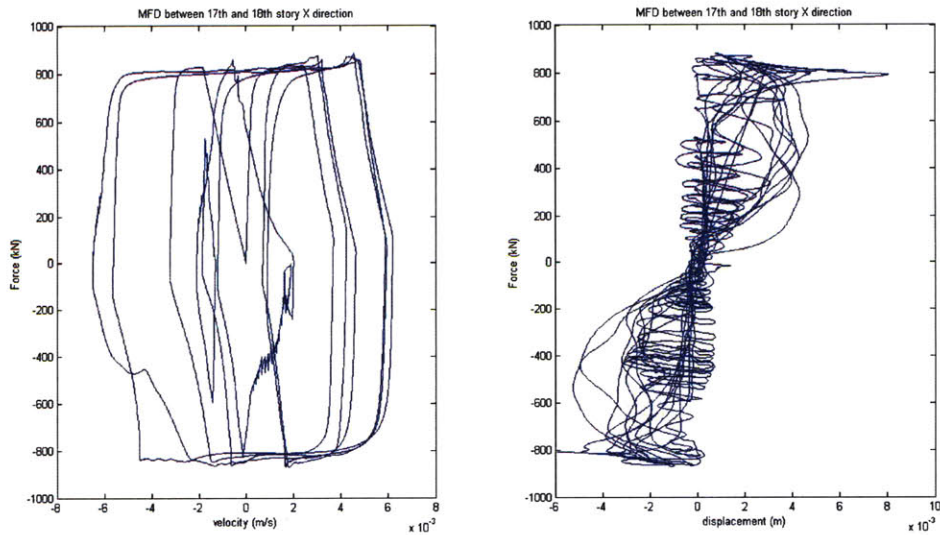


Fig. 42. MFD behavior between 17<sup>th</sup> and 18<sup>th</sup> floor X Direction

Fig. 42 presents a strong friction behavior in the MFD while maintaining a smooth transition in the area of high velocities. In the right hand side, a very interesting hysteretic behavior is presented for MFD between 17 and 18 floor. Maximum capacity of the device is increased up to 800 kN.

#### 6.4.4. 4<sup>TH</sup> ITERATION (800 kN MFD)

		Wind Load Case	
		E-W (X) Dir.	N-S (Y) Dir.
Response without dampers	accel. at 37 <sup>th</sup> Flr.(m/s <sup>2</sup> )	0.64	0.41
	displ. at 37 <sup>th</sup> Flr.(m/s)	0.40	0.28
	Base Shear (kN)	9267	6140
Response with MFD	accel. at 37 <sup>th</sup> Flr.(m/s <sup>2</sup> )	0.43	0.37
	displ. at 37 <sup>th</sup> Flr.(m/s)	0.28	0.25
	Base Shear (kN)	5682	4412

Table 17. Data obtained from the lumped model

Floor	Work X direction (kN*m)	Work Y direction (kN*m)
19	161.6	148.6
21	153.7	138.4
23	176.5	160.7
25	156.9	146.2
27	153.2	107.0

Table 18. Work done by the MFD's

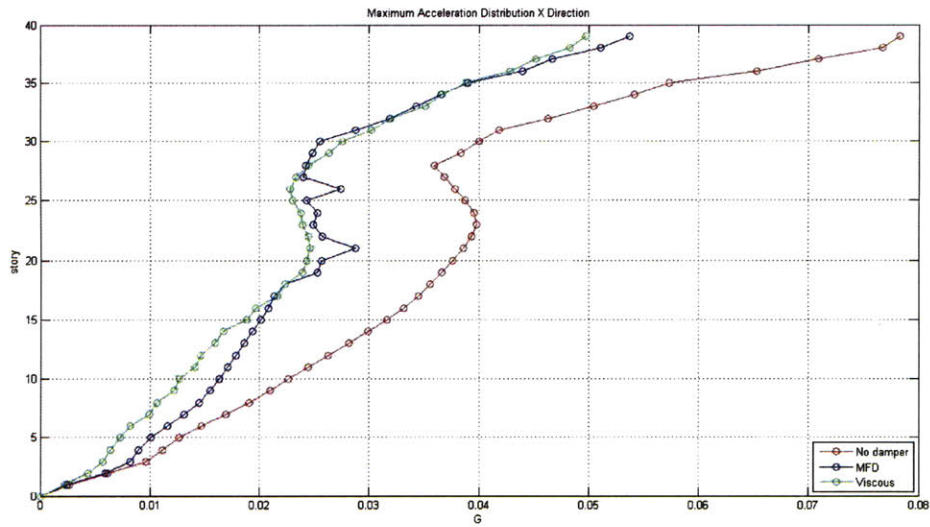


Fig. 43. Data Maximum acceleration profile for X direction

Devices in 15 and 17 stories are removed for this 4<sup>th</sup> iteration (Table 18). MFDs installed in 21 and 25 floor are the most sensitive to acceleration performance. As a result, control is relaxed for both devices. If the last 3 stories are discarded, maximum acceleration of the building is the same for both viscous scheme and MFD scheme (Fig. 43 and Fig. 44). MFD maximum capacity is maintained to 800 kN and the behavior (Fig. 45) is similar to the one observed in the previous iteration.

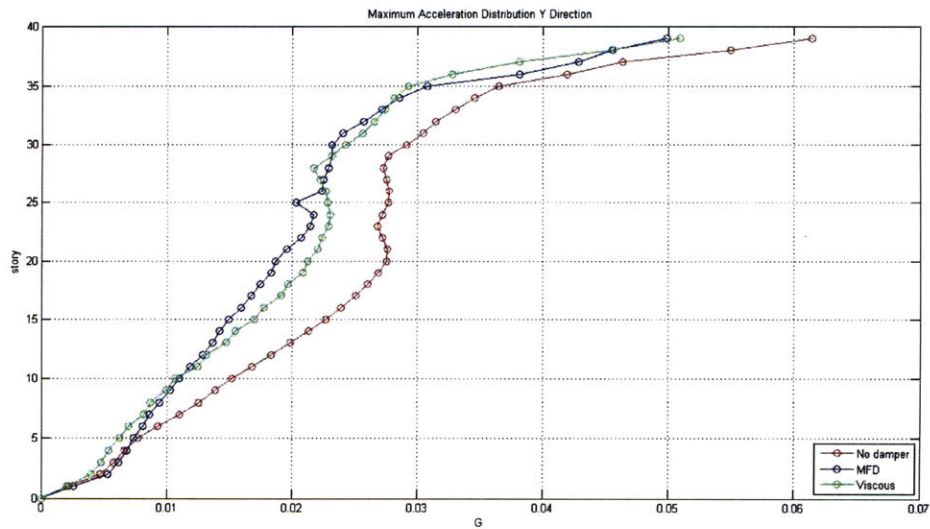


Fig. 44. Data Maximum acceleration profile for Y direction



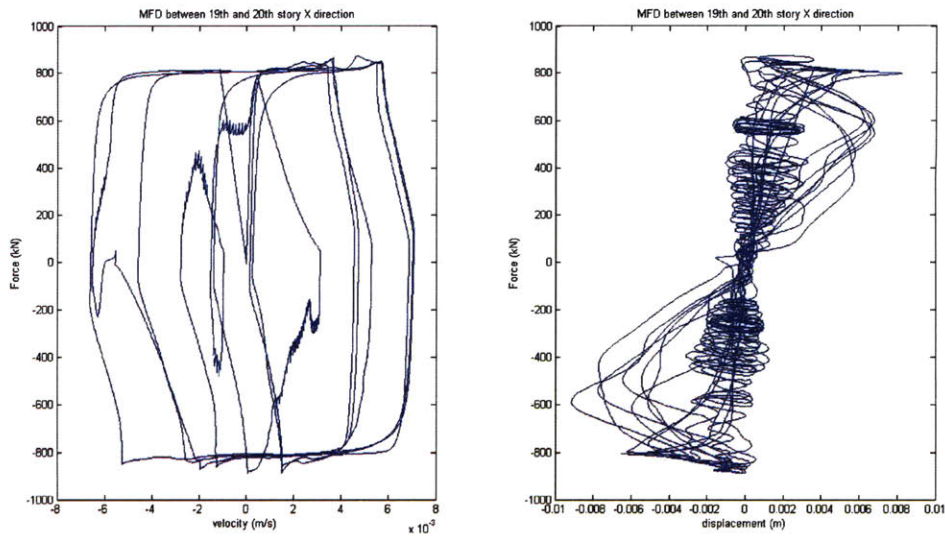


Fig. 45. MFD behavior between 19<sup>th</sup> and 20<sup>th</sup> floor X Direction

6.4.5. 5<sup>TH</sup> ITERATION (1500 kN MFD)

		Wind Load Case	
		E-W (X) Dir.	N-S (Y) Dir.
Response without dampers	accel. at 37 <sup>th</sup> Flr.(m/s <sup>2</sup> )	0.64	0.41
	displ. at 37 <sup>th</sup> Flr.(m/s)	0.40	0.28
	Base Shear (kN)	9267	6140
Response with MFD	accel. at 37 <sup>th</sup> Flr.(m/s <sup>2</sup> )	0.45	0.37
	displ. at 37 <sup>th</sup> Flr.(m/s)	0.29	0.25
	Base Shear (kN)	6102	4532

Table 19. Data obtained from the lumped model

Floor	Work X direction (kN*m)	Work Y direction (kN*m)
19	280.7	212.3
23	213.9	233.6
25	170.7	172.2

Table 20. Work done by the MFD's

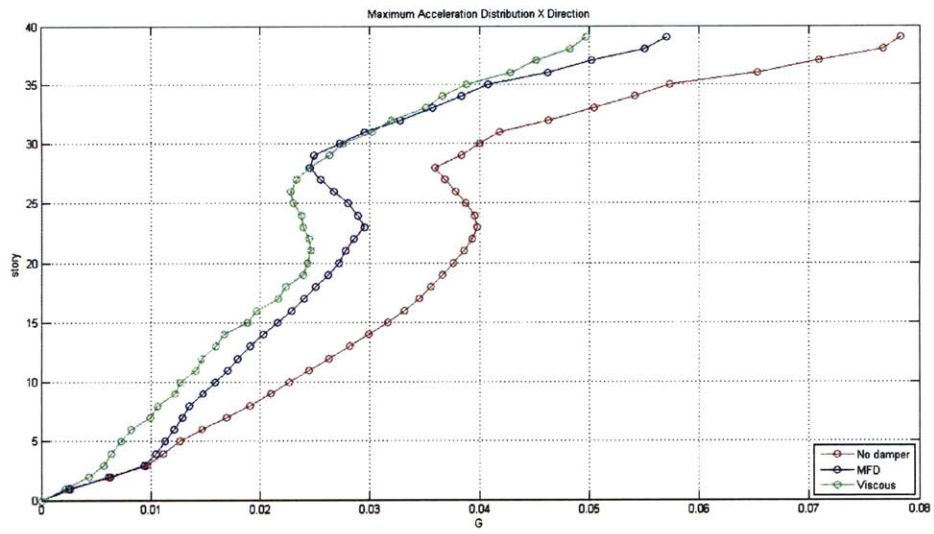


Fig. 46. Data Maximum acceleration profile for X direction

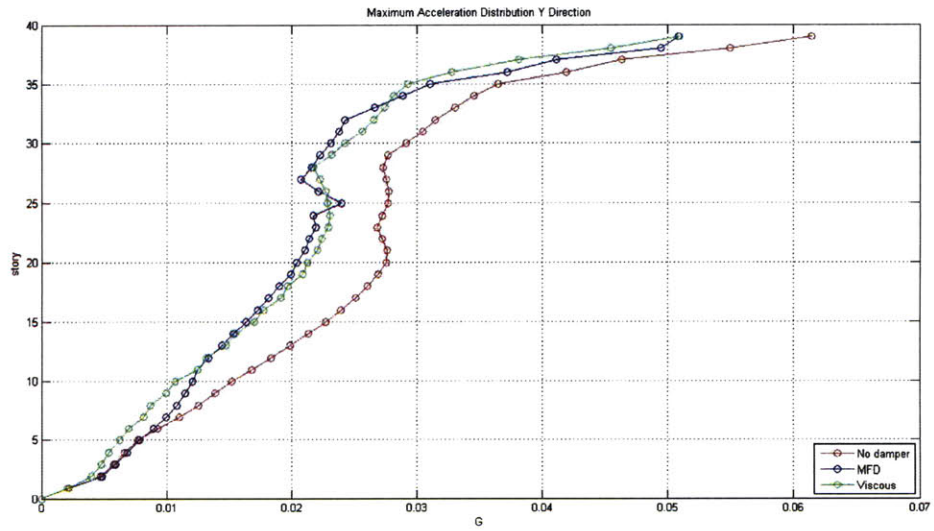


Fig. 47. Data Maximum acceleration profile for Y direction

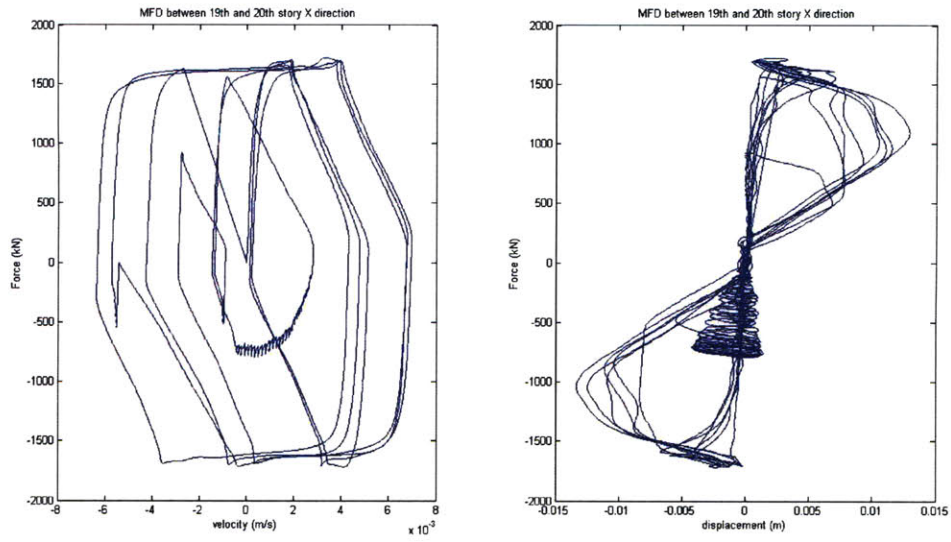


Fig. 48. MFD behavior between 19<sup>th</sup> and 20<sup>th</sup> floor X Direction

For the last iteration, MFDs in stories 21 and 27 are removed (Table 20). Device maximum capacity is chosen to be 1600 kN. Device controller for the 25 floor is critical in the design of the Y direction scheme. Hence, control has been relaxed for this story. Building maximum accelerations obtained with this simple scheme are similar to the ones obtained for the initial viscous damper scheme (Fig. 46 and Fig. 47).

## 7. ECONOMIC EVALUATION

For the economic evaluation, a single viscous damper unit has a value of approximately \$5,000 while MFD is estimated to be \$15,000. However, bracing schemes have a great impact in the final total cost of the implementation. Hence, a basic economic evaluation has to compare every different solution previously presented. Final budgets are summarized in Table 21 and Table 22.

Assuming a total cost of \$1,000,000 for the current solution with viscous dampers and considering that toggle brace system (TBS) has a price 2 times bigger than the simple diagonal frame; unitary prices have been extrapolated for dampers and both bracing systems.

Due to the adaptability of the behavior for semi-active controlled systems. It has not been necessary to use toggle brace systems in the Y Direction. This fact has a direct impact on the final budget of the MFD's solutions because, as previously mentioned, this special bracing has a higher cost than the common diagonal bracing system.

After price for bracing units has been obtained and viscous damper bracing and connections are assumed to be designed to handle up to 300 kN, the cost of the rest of the bracing systems has been assumed to be linearly proportional to the respective device maximum capacity.

		Number of devices	Price per unit	Cost of the devices	Price per bracing	Cost of the the bracing	Total Cost
Viscous dampers	X Direction	30	\$5,000	\$150,000	\$7,778	\$233,333	\$1,000,000
	Y Direction	30	\$5,000	\$150,000	\$15,556	\$466,667	
MFD every 2 stories	X Direction	30	\$15,000	\$450,000	\$4,444	\$133,333	\$1,150,000
	Y Direction	30	\$15,000	\$450,000	\$4,444	\$133,333	
MFD every 4 stories	X Direction	16	\$15,000	\$240,000	\$13,333	\$213,333	\$900,000
	Y Direction	16	\$15,000	\$240,000	\$13,333	\$213,333	
MFD every 6 stories	X Direction	10	\$15,000	\$150,000	\$22,222	\$222,222	\$750,000
	Y Direction	10	\$15,000	\$150,000	\$22,222	\$222,222	
MFD every 8 stories	X Direction	6	\$15,000	\$90,000	\$53,333	\$320,000	\$820,000
	Y Direction	6	\$15,000	\$90,000	\$44,444	\$266,667	

Table 21. Economic evaluation chart for heuristic method

		Number of devices	Price per unit	Cost of the devices	Price per bracing	Cost of the the bracing	Total Cost
Viscous dampers	X Direction	30	\$5,000	\$150,000	\$7,778	\$233,333	\$1,000,000
	Y Direction	30	\$5,000	\$150,000	\$15,556	\$466,667	
MFD 1 <sup>st</sup> iteration	X Direction	24	\$15,000	\$360,000	\$8,889	\$213,333	\$1,150,000
	Y Direction	24	\$15,000	\$360,000	\$8,889	\$213,333	
MFD 2 <sup>nd</sup> iteration	X Direction	18	\$15,000	\$270,000	\$8,889	\$160,000	\$860,000
	Y Direction	18	\$15,000	\$270,000	\$8,889	\$160,000	
MFD 3 <sup>rd</sup> iteration	X Direction	14	\$15,000	\$210,000	\$17,778	\$248,889	\$920,000
	Y Direction	14	\$15,000	\$210,000	\$17,778	\$248,889	
MFD 4 <sup>th</sup> iteration	X Direction	10	\$15,000	\$150,000	\$17,778	\$177,778	\$650,000
	Y Direction	10	\$15,000	\$150,000	\$17,778	\$177,778	
MFD 5 <sup>th</sup> iteration	X Direction	6	\$15,000	\$90,000	\$40,000	\$240,000	\$660,000
	Y Direction	6	\$15,000	\$90,000	\$40,000	\$240,000	

Table 22. Economic evaluation based on the work measurement method

Considering economics and performance for the heuristic method, using MFD's either every 6 stories or 8 stories are the most sensible schemes to follow for the new implementation. However, when work done by every actuator has been considered to remove devices, much better economical solution has been achieved. The final budget for this implementation is reduced by a 45%.

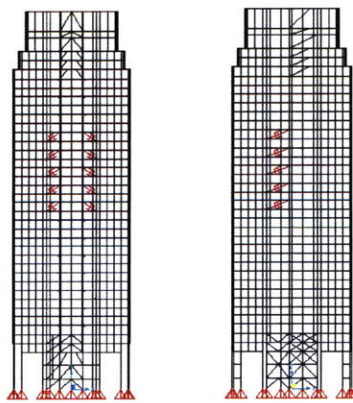


Fig. 49. MFD final layout for X and Y direction.

Final solution consists in 2 MFD's per floor with maximum capacity of 800 kN located in stories 19,21,23,25 and 27 for every direction (X and Y).

## 8. CONCLUSIONS AND FURTHER STUDIES

Implementing MFD's with maximum capacity 200 kN every 2 stories has shown to be very efficient in terms of acceleration reduction under wind excitation. However, because of the assumed higher price of the devices in comparison to the common viscous damper, this solution would result more expensive than the current design.

After reducing the number of devices (every 4, 6 and 8 stories), same performance than wind viscous damper has been achieved. Because of the reduction in number of devices and bracing systems, more economical solutions than the current solution (viscous damper) are achieved. However, this heuristic method based on maintaining the same spacing between dampers has shown to be inefficient. Energy dissipation method has achieved much better solutions in terms of efficiency and economy.

Further studies would include the use of optimization method to select control matrices (see chapter 4). Besides, optimization tools could be used to allocate the MFDs throughout the building (work-based method) in order to optimize the final cost of the implementation. This thesis has used heuristic rules in order to reduce as much as possible the number of devices while maintaining the performance under wind excitations. However, improvement can be done in order to automate the process.

Finally, further studies have to be accomplished in terms of device control and structural behavior when undergoing seismic excitations.

## 9. REFERENCES

Abdellaoui, M. *Study of a Modified Friction Device for the Control of Civil Structures*. Boston: MIT, 2010.

B.F. Spencer, Jr. and T.T. Soong. "New applications and development of active, semiactive and hybrid control techniques for seismic and non-seismic vibration in the USA." *International Post-SMiRT Conference Seminar on Seismic Isolation, Passive Energy Dissipation and Active Control of Vibration of Structures*. Cheju, Korea, 1999.

Choi, S.B. and Lee, S.K. "A hysteresis model for the field-dependent damping force of a magnetorheological damper." *Journal of sound and vibration*, 2001: 375-383.

Connor, J.J. *Introduction to Structural Motion Control*. Boston: Prentice Hall, 2002.

*content.answers.com*.

<http://content.answers.com/main/content/img/McGrawHill/Encyclopedia>.

Dyke, S.J., B.F. Spencer Jr., M.K. Sain and J.D. Carlson. "Reduction, Modeling and Control of Magnetorheological Dampers for Seismic Response." 1996.

Housner, G.W. et al. "Structural control: past, present and future." *Journal of Engineering Mechanics, ASCE*, 1997: 123:897-971.

Huang, R. J. McNamara and C. D. "An Efficient Damper System For High Rise Buildings." 2000.

Laflamme, S., Taylor, D., Abdellaoui Maane, M., and Connor, J. J. "Modified Friction Device for Control of Large-Scale Systems." *In preparation*, 2010.

Larrecq, G. *Heating effects on Magnetorheological damper*. Boston: MIT, 2010.

McNamara, R. and Taylor. "Fluid viscous dampers for high-rise buildings." *the structural design of tall and special buildings*, 2003: 145-154.

McNamara, R. "Viscous-Damper with Motion Amplification Device."

*www.taylordevicesindia.com*. March 15, 2010. <http://www.taylordevicesindia.com> (accessed March 15, 2010).

## APPENDIX A (VISCOUS DAMPER BRACING SCHEME)

Bottom floor	Cx(kN/m*s)	Cy(kN/m*s)	No dampers X	No dampers Y	Amplification factor X	Amplification factor Y	Max stroke wind X (kN)	Max stroke seismic X (kN)
5	52535	3502	2	2	0.70	7.16	721	2807
7	52535	3502	2	2	0.70	7.16	721	2807
9	52535	3502	2	2	0.70	7.16	721	2807
11	52535	3502	2	2	0.70	7.16	721	2807
13	52535	3502	2	2	0.70	7.16	721	2807
15	52535	3502	2	2	0.70	7.16	738	3056
17	52535	3502	2	2	0.70	7.16	738	3056
19	52535	3502	2	2	0.70	7.16	738	3056
21	52535	3502	2	2	0.70	7.16	738	3056
23	52535	3502	2	2	0.70	7.16	738	3056
25	52535	3502	2	2	0.70	7.16	627	2482
27	35024	1751	2	2	0.70	7.16	627	2482
29	35024	1751	2	2	0.70	7.16	627	2482
31	35024	1751	2	2	0.70	7.16	627	2482
33	35024	1751	2	2	0.70	7.16	627	2482
Bottom floor	Max stroke wind Y (kN)	Max stroke seismic Y (kN)	Cx total (kN/m*s)	Cy total (kN/m*s)	Max stroke wind X (kN)	Max stroke seismic X (kN)	Max stroke wind Y (kN)	Max stroke seismic Y (kN)
5	160	712	73904	50165	604	2354	850	3778
7	160	712	73904	50165	604	2354	850	3778
9	160	712	73904	50165	604	2354	850	3778
11	160	712	73904	50165	604	2354	850	3778
13	160	712	73904	50165	604	2354	850	3778
15	151	712	73904	50165	619	2563	803	3778
17	151	712	73904	50165	619	2563	803	3778
19	151	712	73904	50165	619	2563	803	3778
21	151	712	73904	50165	619	2563	803	3778
23	151	712	73904	50165	619	2563	803	3778
25	71	587	73904	50165	526	2082	378	3117
27	71	587	49269	25082	526	2082	378	3117
29	71	587	49269	25082	526	2082	378	3117
31	71	587	49269	25082	526	2082	378	3117
33	71	587	49269	25082	526	2082	378	3117



## APPENDIX B (BUILDING STRUCTURAL PROPERTIES)

Story	Kx (kN/m)	Mx (tons)	Cx (kN*s <sup>2</sup> /m)	Ky (kN/m)	My (tons)	Cy (kN*s <sup>2</sup> /m)	Krot (kN*m)	Mrot (tons*m <sup>2</sup> )	Crot (kN*s <sup>2</sup> *m)
1	2067074	1671	29945	2193660	1671	31776	799352942	1374428	11599849
2	1505673	3150	21865	2751949	3150	39892	658901400	7278970	9728490
3	2549942	2295	36947	3929345	2295	56900	1315145346	3529531	19119217
4	3611396	1394	52276	3919347	1394	56731	1848721007	1039067	26769731
5	3101010	1394	44894	3226434	1394	46708	1750468891	1039067	25348526
6	2474746	1482	35837	2662444	1482	38552	1711792409	1121533	24791314
7	2350774	948	34029	2615282	948	37855	1774176724	368347	25673253
8	2320532	948	33592	2579392	948	37336	1772923676	368347	25655128
9	2291418	948	33171	2536604	948	36717	1770888973	368347	25625696
10	2058960	948	29808	2283559	948	33057	1676228490	368347	24256443
11	1825557	948	26432	2024855	948	29315	1581327973	368347	22883719
12	1803505	948	26113	1987942	948	28781	1579171181	368347	22852521
13	1778835	948	25756	1954807	948	28302	1576948326	368347	22820368
14	1668297	948	24157	1848105	948	26758	1483770449	368347	21472561
15	1569127	948	22723	1736539	948	25145	1390477722	368347	20123092
16	1545882	948	22387	1704402	948	24680	1387921322	368347	20086114
17	1521633	948	22036	1671516	948	24204	1385375108	368347	20049284
18	1419114	948	20553	1542103	948	22332	1278272863	368347	18500062
19	1307801	948	18943	1414101	948	20481	1171095906	368347	16949761
20	1286285	948	18632	1385321	948	20064	1168968039	657762	16926836
21	1269242	948	18385	1370469	948	19849	1166888612	657762	16896758
22	1137804	948	16484	1216329	948	17620	1054584571	657762	15272293
23	1004400	948	14554	1064386	948	15422	942203178	657762	13646710
24	989713	948	14342	1049687	948	15209	940368734	657762	13620174
25	976682	948	14153	1030839	948	14937	938594029	657762	13594504
26	902145	948	13075	959764	948	13909	881514404	657762	12768854
27	833167	948	12077	889946	948	12899	824415005	657762	11942918
28	826925	948	11987	880965	948	12769	822486957	657762	11915029
29	810376	948	11748	866126	948	12554	820582427	657762	11887480
30	743926	948	10787	788614	948	11433	754998730	657762	10938819
31	690218	948	10010	721919	948	10468	689375175	657762	9989582
32	672214	948	9749	707994	948	10267	688006358	657762	9969783
33	655784	948	9512	688855	948	9990	686683441	657762	9950647
34	647633	948	9394	668236	948	9692	657964874	657762	9535236
35	411402	948	5977	429995	948	6246	377108923	657762	5472688
36	208452	804	3037	200943	804	2928	128495774	479086	1871679

Story	Kx (kN/m)	Mx (tons)	Cx (kN*s <sup>2</sup> /m)	Ky (kN/m)	My (tons)	Cy (kN*s <sup>2</sup> /m)	Krot (kN*m)	Mrot (tons*m <sup>2</sup> )	Crot (kN*s <sup>2</sup> *m)
37	188644	984	2755	144156	984	2112	90540972	539954	1324319
38	127547	903	1869	61570	903	915	36349515	318278234	9164241
39	53342	125	775	13206	125	194	11812546	196347	176196